TDP-43 prevents endogenous RNAs from triggering a lethal RIG-I-dependent interferon response

William Dunker[1], **Xiang Ye**[1], **Yang Zhao**[1], **Lanxi Liu**[1], **Antiana Richardson**[1], **John Karijolich**[1,2,3,4,5,*]

[1]Department of Pathology, Microbiology, and Immunology, Vanderbilt University Medical Center, Nashville, TN 37232-2363, USA

[2]Department of Biochemistry, Vanderbilt University School of Medicine, Nashville, TN 37232-2363, USA

[3]Vanderbilt-Ingram Cancer Center, Nashville, TN 37232-2363, USA

[4]Vanderbilt Institute for Infection, Immunology and Inflammation, Nashville, TN 37232-2363, USA

[5]Vanderbilt Center for Immunobiology, Nashville, TN 37232-2363, USA

SUMMARY

RIG-I-like receptors (RLRs) are involved in the discrimination of self versus non-self via the recognition of double-stranded RNA (dsRNA). Emerging evidence suggests that immunostimulatory dsRNAs are ubiquitously expressed but are disrupted or sequestered by cellular RNA binding proteins (RBPs). TDP-43 is an RBP associated with multiple neurological disorders and is essential for cell viability. Here, we demonstrate that TDP-43 regulates the accumulation of immunostimulatory dsRNA. The immunostimulatory RNA is identified as RNA polymerase III transcripts, including 7SL and *Alu* retrotransposons, and we demonstrate that the RNA-binding activity of TDP-43 is required to prevent immune stimulation. The dsRNAs activate a RIG-I-dependent interferon (IFN) response, which promotes necroptosis. Genetic inactivation of the RLR-pathway rescues the interferon-mediated cell death associated with loss of TDP-43. Collectively, our study describes a role for TDP-43 in preventing the accumulation of endogenous immunostimulatory dsRNAs and uncovers an intricate relationship between the control of cellular gene expression and IFN-mediated cell death.

In brief

Dunker et al. report that TDP-43 is involved in the regulation of immunostimulatory double-stranded RNA (dsRNA) homeostasis. TDP-43 associates with select RNA polymerase III

transcripts, and its loss results in their increased expression and detection by RIG-I. This study furthers our understanding of intrinsic mechanisms regulating immunostimulatory dsRNA accumulation.

Graphical Abstract
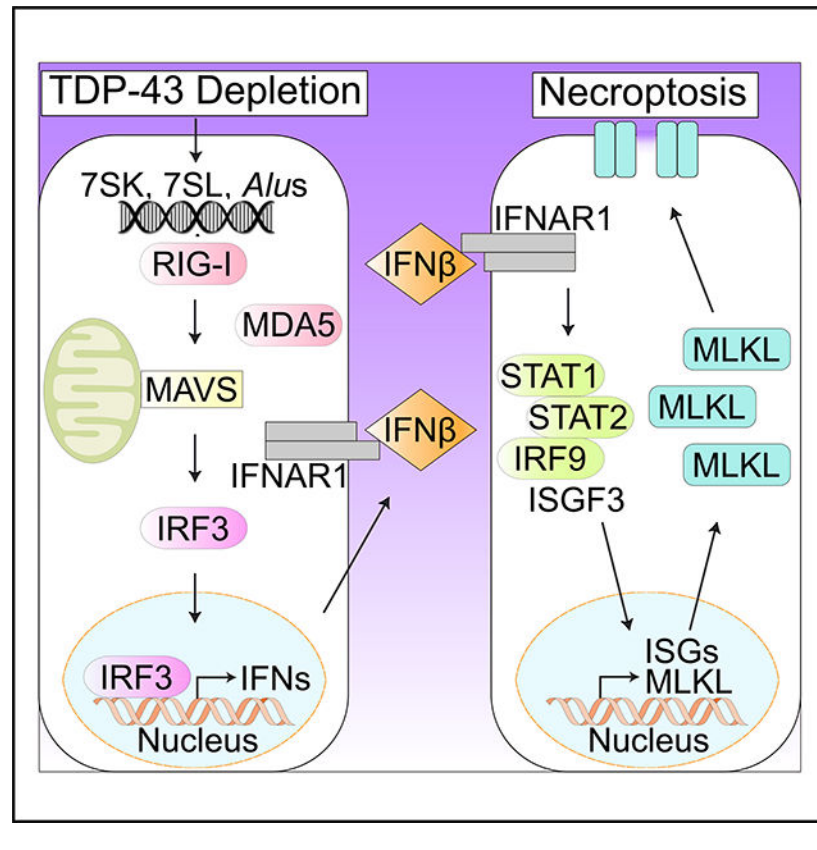
INTRODUCTION

The regulation of innate immune double-stranded RNA (dsRNA) sensors is paramount for initiating a robust antimicrobial gene expression response as well as for preventing an aberrant immune response to endogenous dsRNA. The primary cell-intrinsic dsRNA sensors include the RIG-I-like receptors (RLRs), Toll-like receptor 3 (TLR3), protein kinase R (PKR), and the $2'-5'$-oligoadenylate synthetase (OAS) proteins (Bou-Nader et al., 2019; Choi et al., 2015; Kawasaki and Kawai, 2014; Loo and Gale, 2011; Reikine et al., 2014). Activation of these receptors induces an antimicrobial gene-expression response, including the production of interferon (IFN) and other proinflammatory cytokines.

The RLR family members retinoic acid-inducible gene I (RIG-I) and melanoma differentiation-associated protein 5 (MDA5) recognize distinct structural and chemical moieties of RNAs. For example, RIG-I preferentially recognizes short (<1,000 bp) $5'$-triphosphorylated ($5'$ppp) blunt dsRNAs, although it can also recognize $5'$ppp single-stranded RNA (ssRNA) and circular RNAs at a lower affinity (Chen et al., 2017; Hornung et

al., 2006; Kato et al., 2008; Pichlmair et al., 2006; Rehwinkel et al., 2010; Schlee et al., 2009; Schmidt et al., 2009). Conversely, MDA5 binds long (>1,000 bp) dsRNA independent of 5′-end phosphorylation status (Kato et al., 2008, 2006). Activation of either receptor drives their association with the adaptor protein mitochondrial antiviral-signaling (MAVS) protein. Signaling through MAVS proteins promotes the activation and nuclear translocation of the transcription factor complexes IFN regulatory factor (IRF) and nuclear factor κ-light-chain-enhancer of activated B cells (NF-κB), resulting in the expression of IFNs and cytokines (Loo and Gale, 2011; Reikine et al., 2014).

Immunostimulatory dsRNAs are generally not present within the host transcriptome because their presence would activate an IFN gene expression response potentially resulting in lethality. To circumvent their production, cells employ a diverse collection of incompletely understood mechanisms. Recent studies have identified RNA-binding proteins (RBPs) that regulate essential junctions of RNA biogenesis, whose deletion results in dsRNA sensor activation. For example, depletion of heterogenous ribonucleoprotein (hnRNP) C, which regulates pre-mRNA splicing through the binding of proximal *Alu* elements, results in RIG-I-dependent cell death from the generation of dsRNA hairpins formed between inverted *Alu* repeats (König et al., 2010; Wu et al., 2018; Zarnack et al., 2013). Additionally, adenosine deaminase RNA-specific (ADAR) enzymes recognize and deaminate adenosine to inosine within dsRNA, generating imperfect dsRNA structures, and loss of that activity results in RLR-dependent sensing of endogenous dsRNA (Kim et al., 1994; Liddicoat et al., 2015; Mannion et al., 2014; Melcher et al., 1996; Nishikura et al., 1991; Pestal et al., 2015). These connections between RBPs and RLR-dependent innate responses hint toward a deep connection between the proper control of gene expression and cell-intrinsic immune mechanisms.

TAR-DNA-binding-protein 43 (TDP-43) is an RNA-binding protein that participates in multiple steps of RNA metabolism, including transcription, splicing, and transport of mRNA, as well as microRNA metabolism (Alami et al., 2014; Buratti and Baralle, 2012; Chung et al., 2018; Kawahara and Mieda-Sato, 2012; Lalmansingh et al., 2011; Polymenidou et al., 2011; Tollervey et al., 2011). The misregulation of RNA processing has been described in a growing number of neurological diseases, and TDP-43 is implicated in amyotrophic lateral sclerosis (ALS) and frontotemporal lobar dementia (FTLD) (Vanden Broeck et al., 2014; Prasad et al., 2019). However, the mechanisms by which TDP-43 contributes to disease are not completely understood.

Many of the TDP-43-associated functions involve dsRNA structures, whether as products or as intermediates. Along that line, previous work has demonstrated that the loss of the TDP43 homolog, TDP-1, in *Caenorhabditis elegans*, and small interfering RNA (siRNA) depletion of TDP-43 in HeLa and M17 neuroblastoma cells result in dsRNA accumulation (Saldi et al., 2014; Shelkovnikova et al., 2018). However, the physiological relevance of these dsRNAs is unknown. Given the prominence of dsRNAs as activators of RLR-dependent IFN responses, we sought to investigate whether TDP-43 is required to prevent the activation of an RLR response to endogenous RNAs. Here, we demonstrate that loss of TDP-43 induces cytoplasmic immunostimulatory dsRNA accumulation triggering a RIG-dependent type-I and -III IFN response. RIG-I activation is driven in part by the upregulation and

mislocalization of TDP-43-bound RNA polymerase III (RNAPIII) transcribed noncoding RNAs, including *Alu* retrotransposons. Moreover, we demonstrate that cell death associated with the loss of TDP-43 can be prevented by CRISPR-Cas9 knockout (KO) of either the RLR pathway or the type-I IFN receptor IFNAR1. IFN signaling induces expression of the pore-forming protein mixed-lineage kinase-domain-like pseudokinase (MLKL), leading to cell death, thus, uncovering a link between RBP-mediated control of gene expression and necroptosis. Collectively, our study describes a role for TDP-43 in preventing the accumulation of endogenous, immunostimulatory dsRNAs and uncovers an intricate relationship between the control of cellular gene expression and IFN-mediated cell death.

RESULTS

Loss of TDP-43 is associated with the accumulation of immunostimulatory dsRNA

Knockdown of TDP-43 in HeLa and M17 neuroblastoma cells results in dsRNA accumulation (Saldi et al., 2014; Shelkovnikova et al., 2018). However, their effect on cellular homeostasis has yet to be determined. Given that dsRNA can serve as a potent activator of a cell-intrinsic IFN response, we hypothesized that the loss of TDP-43 would result in the accumulation of immunostimulatory dsRNA. To test that, we depleted TDP-43 using siRNA in the SH-SY5Y neuroblastoma cell line and analyzed dsRNA accumulation 48 h after knockdown by immunofluorescence (IF) microscopy using the J2 dsRNA-specific antibody. The J2 antibody is commonly used to visualize and isolate dsRNA because it recognizes RNA helices equal or greater than 40 bp in a sequence-independent manner (Weber et al., 2006). Poly(I:C), a synthetic analog of dsRNA, was transfected as a positive control. Consistent with previous results in HeLa and M17 cells, TDP-43 depletion in SH-SY5Y cells resulted in dsRNA accumulation when compared with the nontarget siRNA (siCON)-treated cells (Figure 1A). The J2+ dsRNA was only observed in the cytoplasm.

To determine whether the dsRNA is immunostimulatory, we performed J2 or control immunoglobulin G (IgG) immunoprecipitations (IPs) on total RNA extracted from cells treated with either siCON or siTDP-43 and transfected the immunopurified RNAs into a reporter cell line, followed by quantification of IFN-β mRNA levels by qRT-PCR (Figures 1B and 1C). Although transfections of RNA purified by the control IgG did not induce IFN-β, regardless of siRNA treatment, J2-purified RNAs from siTDP-43-treated cells resulted in a significant increase in IFN-β expression when compared with siCON-treated cells (Figure 1C). Additionally, removal of the 5′ phosphate structures with calf-intestinal alkaline phosphatase (CIAP) treatment prevented IFN-β induction.

Given that the J2 IP enriched immunostimulatory dsRNA, we next sought to determine whether depletion of TDP-43 resulted in the induction of an IFN-gene-expression response. SH-SY5Y cells were treated with siCON or siTDP-43 for 48 h before RNA extraction and quantification of IFN expression (Figures 1D and 1E). As a positive control, we transfected poly(I:C). TDP-43 depletion resulted in expression of the type-I IFN, IFN-β, and the type-III IFNs, IFN-λ1 and −2/3 (Figure 1E). In contrast, the type-I IFN, IFN-α, and type-II IFN, IFN-γ, were not induced. These results mirror the IFN expression profile upon poly(I:C) transfection. To further assess the effects of TDP-43 depletion on gene expression, we quantified the expression of several IFN-stimulated genes (ISGs) as well as downstream

targets of NF-κB. TDP-43 knockdown induced expression of several ISGs (Figure 1F). Interestingly, although poly(I:C) induced the expression of multiple NF-κB targets, knockdown of TDP-43 did not (Figure 1G).

We next sought to investigate whether the IFN response that was associated with the loss of TDP-43 was neuronal specific or was also observed in cell lines derived from other tissue. To test that, 786-O clear cell renal cell carcinoma (ccRCC) cells were transfected with siCON or siTDP-43, and the IFN-gene-expression response was quantified by qRT-PCR. Importantly, we observed that loss of TDP-43 induced an IFN and ISG expression profile identical to that observed in SH-SY5Y cells (Figures S1A–S1D). Collectively, these results demonstrate that the loss of TDP-43 results in the accumulation of dsRNA, which activates an IFN-gene-expression response.

TDP-43 knockdown activates a RIG-I-dependent immune response

To test whether the IFN response was dependent on RLR signaling, we generated CRISPR-Cas9 KOs of the essential RLR components MAVS, RIG-I, and MDA5 in the SH-SY5Y cell line (Figures 2A–2C). Full-length (FL) and truncated (mini) MAVS isoforms can regulate an immune response; thus, guide RNAs were designed to target both isoforms (Biacchesi et al., 2009; Hou et al., 2011). Western blot analysis confirmed KO of both FL and mini MAVS (Figure 2B). RIG-I and MDA5 are IFN-inducible proteins; thus, depletion of TDP-43 induced their expression in wild-type (WT) cells but not in the KO cell lines (Figure 2C). We further validated the KOs by identifying the CRISPRCas9-induced mutations by Sanger sequencing of the genomic loci from single-cell clones (Table S2).

To investigate the IFN response, we treated the WT and KO cells with siCON or siTDP-43 for 48 h and quantified IFN and ISG gene expression by qRT-PCR (Figures 2D and 2E). Although siTDP-43 resulted in robust IFN and ISG expression in WT and MDA5 KO cells, their expression was completely abrogated in both MAVS and RIG-I KOs (Figures 2D and 2E). These results suggest that TDP-43 depletion induces a RIG-I-dependent IFN response.

To rule out potential off-target effects of the RIG-I single-guide RNA (sgRNA), we complemented the RIG-I KO with a doxycycline (DOX)-inducible guide RNA-resistant FLAG-tagged RIG-I and evaluated the IFN response in cells transfected with siCON or siTDP-43 (Figures 2F and 2G). Western blot analysis confirmed that DOX treatment resulted in FLAG-RIG-I expression (Figure 2F). Consistent with a requirement for RIG-I in sensing the accumulated dsRNA, IFN-β expression was only observed in cells treated with DOX and siTDP-43 (Figure 2G). To determine whether RIG-I was similarly required for the IFN response in 786-O cells, we generated MAVS, RIG-I, and MDA5 KO cells and quantified IFN and ISG expression by qRT-PCR in siCON and siTDP-43-treated 786-O cells. Consistent with results obtained in the SH-SY5Y cells, IFN and ISG expression was only observed in WT and MDA5 cells (Figures S2A–S2G).

We further investigated the effect of dsRNA accumulation in HEK293T cells because they do not express RIG-I. To test the dependency of the IFN response on RIG-I in HEK293T cells, we generated cells harboring a DOX-inducible FLAG-RIG-I. Culturing of HEK293T cells harboring the DOX-inducible RIG-I transgene (iRIG-I cells) revealed leaky RIG-I

expression (Figure 2H). RIG-I ligand transfection demonstrated that WT HEK293T cells do not mount an IFN response, whereas leaky RIG-I expression in iRIG-I cells was sufficient for IFN-β induction (Figure 2I). WT and iRIG-I cells were then treated with siCON or siTDP-43 for 48 h and IFN-β expression was quantified by qRTPCR (Figure 2J). Consistent with a role for RIG-I sensing the accumulated dsRNA, IFN-β was only observed in siTDP-43treated iRIG-I cells. Collectively, these results demonstrate that loss of TDP-43 activates a RIG-I-dependent IFN response.

Lastly, to determine whether the IFN expression resulted in a functional antiviral response, we treated SH-SY5Y and 786-O cells with siCON or siTDP-43 for 48 h, followed by infection with Kaposi's sarcoma-associated herpesvirus (KSHV), an oncogenic DNA herpesvirus (Giffin and Damania, 2014) The abundance of the KSHV transcript LANA (latency-associated nuclear antigen) was used to quantify infection. Loss of TDP-43 significantly reduced LANA levels compared with that of siCON-treated cells (Figures S3A and 3B). Importantly, TDP-43 depletion in the MAVS KO cell lines did not reduce LANA abundance, demonstrating that it is an antiviral IFN response and not TDP-43 regulating KSHV infection.

IRF3 is required for the IFN and ISG response observed in TDP-43-depleted cells

RIG-I activation of an IFN response canonically proceeds through the adaptor protein MAVS, which further recruits and activates the transcription factor IFN regulatory factor 3 (IRF3). We generated a 15 bp, in-frame deletion of IRF3 in SH-SY5Y cells, which prevents it from activating IFN expression after transfection of a RIG-I ligand (Figures 3A and 3B; Table S2). To investigate the role of IRF3, we transfected WT or truncated IRF3 SH-SY5Y cells with siCON or siTDP-43 and quantified IFN and ISG expression by qRT-PCR. Although TDP-43 depletion in WT cells resulted in a robust IFN and ISG response, inactivation of IRF3 completely prevented IFN and ISG expression (Figures 3C and 3D). Moreover, we generated an IRF3 KO in 786-O cells and observed a similar requirement for IRF3 in the IFN and ISG response (Figures S4A–S4E). Collectively, these data demonstrate that the loss of TDP-43 activates a RIG-I-, MAVS-, and IRF3-dependent types-I and -III IFN response.

TDP-43 knockdown increases the levels of multiple RNAPIII RNAs

We next sought to determine how loss of TDP-43 affects cellular gene expression. Leveraging RNA sequencing, we defined the transcriptome of FLAG-RIG-I complemented RIG-I KO SH-SY5Y cells treated with either siCON or siTDP-43 (Figure 4A). Differential gene expression analysis revealed two distinct clusters of up- and downregulated genes (Figure 4B; Table S3). Although multiple ontological terms are present within these clusters, many of the most significant terms present among the upregulated genes are involved in RNAPIII transcription (Tables S4 and S5). RNAPIII transcribes housekeeping, noncoding RNAs, such as tRNAs and a variety of small non-coding RNAs, including 7SK snRNA (RN7SK), 7SL RNA (RN7SL), and *Alu* retrotransposons, which are in the short interspersed repetitive elements (SINEs) class of retrotransposons (White, 2011). Aberrant expression of RNAPIII transcripts, including 7SL and *Alu* RNAs, has previously been shown to activate a RIG-I-dependent IFN response (Nabet et al., 2017; Wu et al., 2018). Inspection of our RNA-

sequencing data revealed that, indeed, the 7SK snRNA, 7SL RNA, and H1 RNA components of RNase P were expressed significant more in cells depleted of TDP-43, and qRT-PCR further confirmed those findings (Figures 4C and 4D). Additionally, *Alu* loci with clear, increased expression were identified, and qRT-PCR analysis confirmed their increased expression. Because *Alu* elements are frequently located within introns and untranslated regions of mRNA, we also assessed the expression of independently transcribed *Alu* RNA by northern blot analysis using an oligonucleotide directed at a consensus *Alu* motif. Consistent with our previous analyses, using the consensus *Alu* motif oligonucleotide, we observed increased expression of an RNA migrating at ~300 nt, the expected length of independently transcribed *Alu* RNA (Figures 4D–4F).

Using previously published TDP-43 individual-nucleotide resolution UV-crosslinking and immunoprecipitation (iCLIP) sequencing data, we observed that many of the upregulated RNAPIII transcripts have prominent TDP-43 iCLIP tags near their 3′ end (Figure 4F) (Tollervey et al., 2011). To verify the iCLIP data, we performed IPs using either anti-TDP-43 or control-IgG antibodies and quantified the enrichment of 7SK, 7SL, and a consensus *Alu* sequence (Figures 4G and 4H). Consistent with the iCLIP data, we observed a significant enrichment of all three RNAPIII transcripts over the control IgG (Figure 4H).

Although TDP-43 has not been associated with the regulation of RNAPIII transcript stability, it has been linked to the regulation of mRNA half-life. Thus, we investigated whether the increased expression of select RNAPIII transcripts was due to alterations in RNA half-life. To test that, we determined the half-life of 7SL RNA and a control RNAPIII transcript, vault RNA 1–1, which did not exhibit increased expression in TDP-43-depleted cells. Loss of TDP-43 extended the half-life of 7SL RNA, whereas the half-life of vault RNA was not affected (Figure 4I). We next investigated whether TDP-43 RNA binding was necessary for regulating 7SL RNA half-life. To test that, we generated HEK293T TDP-43 KO cells and transfected them with either an empty vector, WT TDP-43, or an RNA-binding, defective TDP-43 (mutRRM; W113A/R151A) (Figure 4J). Although expression of WT TDP-43 reduced 7SL half-life relative to the empty-vector control, the half-life of 7SL RNA was not altered by expression of the RNA-binding, defective TDP-43 (Figure 4K). These results demonstrate a role for TDP-43 in the regulation of select RNAPIII transcript stability and suggest this contributes to changes in the transcriptome in TDP-43-depleted cells.

We also examined the nuclear/cytoplasmic localization of the TDP-43-bound RNAPIII transcripts by qRT-PCR because TDP43 has previously been linked to nuclear export of mRNA (Chou et al., 2018). After whole-cell fractionation into nuclear and cytoplasmic fractions, we observed a significant cytoplasmic relocalization of the primarily nuclear 7SK snRNA in TDP-43-depleted cells (Figures 4L and 4M). Moreover, although *Alu* and 7SL RNAs are normally present in the cytoplasm, we observed an increase in cytoplasmic levels of both RNAs (Figure 4M). Collectively, these results demonstrate that TDP-43 affects the expression, localization, and decay of select RNAPIII-transcribed RNAs.

RNAPIII RNAs are associated with and activate RIG-I upon loss of TDP-43

7SL and *Alu* RNAs have previously been demonstrated to activate a RIG-I-dependent IFN response (Nabet et al., 2017; Wu et al., 2018). To test whether RNAPIII transcription is required to promote activation of RIG-I upon loss of TDP-43, we treated cells with siCON or siTDP-43 in the presence of an RNAPIII-specific inhibitor and assessed the IFN-β expression by qRT-PCR. Inhibition of RNAPIII transcription was confirmed by measuring the levels of cellular vault RNA 1–1 (Figure 5A). Strikingly, inhibition of RNAPIII transcription completely prevented the induction of IFN-β expression when TDP-43 was depleted (Figure 5A). These results indicate that RNAPIII transcription is required for activating RIG-I.

Next, we tested whether TDP-43 RNA binding was required to prevent IFN-β expression. HEK293T TDP-43 KO cells were co-transfected with RIG-I and either an empty vector, WT TDP-43, or an RNA-binding, defective TDP-43 (mutRRM; W113A/R151A), and IFN-β expression was quantified by qRTPCR (Figures 5B and 5C). Supporting our evidence that RIG-I is required to sense dsRNA that accumulates when TDP-43 is absent we observed IFN β expression in TDP-43 KOs transfected with RIG-I and an empty vector (Figure 5C). Furthermore, we observed IFN β expression in cells that expressed RNA-binding defective TDP-43 whereas expression of WT TDP-43 rescued IFN β expression. These data demonstrate that the RNA-binding capacity of TDP-43 is required to prevent IFN β expression.

As our data implicate RNAPIII activity as well as the ability of TDP-43 to bind RNA in the induction of IFN β expression we evaluated whether RIG-I interacts with TDP-43-target RNAs by IPqRT-PCR (Figures 5D and 5E). TDP-43 knockdown resulted in an increased association between RIG-I and several of its RNAPIII transcribed RNA binding partners, including 7SK snRNA, 7SL RNA, and *Alu* RNA (Figure 5E). In contrast, the binding of RIG-I to TDP-43 associated spliceosomal snRNAs, noncoding RNAs, and mRNAs were not affected by TDP-43 depletion (Figure 5E). These results demonstrate that loss of TDP-43 facilitates RIG-I recognition of select RNAPIII-transcribed RNAs that can be bound by TDP-43.

A defining feature of many RIG-I substrates is the presence of a 5′-triphosphate. Dual-specificity phosphatase 11 (DUSP11) is an RNA triphosphatase that acts on several RNAPIII-derived RNAs, and a reduction in its activity has been shown to activate a RIG-I-dependent IFN response (Burke et al., 2016; Burke and Sullivan, 2017; Zhao et al., 2018). Although we did not observe a reduction in DUSP11 expression in our transcriptomic data, we hypothesized the significant increase in RNAPIII RNA levels may result in some transcripts escaping the activity of DUSP11 thus enabling their engagement by RIG-I. To test that, we transduced SH-SY5Y cells with a DOX-inducible DUSP11 transgene and quantified IFN expression in siCON- and siTDP-43-depleted cells (Figures 5F and 5G). Consistent with our previous observations, knockdown of TDP-43 resulted in the expression of IFN-β mRNA when cells were grown in the absence of DOX (Figure 5G). Although we still observed IFN-β mRNA expression when DUSP11 was overexpressed, we observed a ~50% reduction in IFN-β mRNA levels, indicating that some of the immunostimulatory RNAs are triphosphorylated. Together, these data demonstrate that select RNAPIII

transcripts are associated with RIG-I upon TDP-43 depletion and reveal a role for TDP-43 in limiting the accumulation of triphosphorylated RNAs.

Genetic inactivation of the RLR pathway rescues the IFN-mediated cell death associated with loss of TDP-43

Cell culture and animal models have demonstrated that TDP-43 is essential for viability, and multiple mechanisms have been proposed, including the dysregulation of Rho family GTPases, an accumulation of dsDNA breaks, and defects in autophagy (Bose et al., 2011; Iguchi et al., 2009; Kraemer et al., 2010; Mitra et al., 2019; Schmid et al., 2013). Based on our observations, we hypothesized that TDP-43 depletion induced an immune-mediated cell death. To test that, we treated SH-SY5Y WT, RIG-I KO, MDA5 KO, MAVS KO, and IRF3-truncation cells with either siCON or siTDP-43 and measured cell viability 5 days after transfection by trypan blue staining and ATP production using a Cell-Titer-Glo assay (Figures 6A and 6B). TDP-43 knockdown reduced cell viability and ATP production in WT and MDA5 KO cells (Figures 6A and 6B). In contrast, in MAVS and RIG-I KOs, and IRF3-truncation cells, depletion of TDP-43 did not reduce cell viability or ATP production when compared with siCON treatment. (Figures 6A–6D). Importantly, TDP-43 depletion-mediated cell death was also rescued in the 786-O MAVS KO, RIG-I KO, and IRF3 KO cells (Figure S5A–S5D).

Because inactivation of IRF3 rescued cell death, we hypothesized that the IRF3-dependent type-I or -III IFNs induce cell death via signaling through either the IFN-α/β receptor 1 (IFNAR1) or IFN-λ receptor 1 (IFNLR1), respectively. qRT-PCR analysis determined that IFNAR1 was expressed at significantly higher levels than IFNLR1 was in both SH-SY5Y and 786-O cells (Figure 6E; Figure S5E). To test whether signaling through IFNAR1 contributed to the cell-death phenotype, we generated IFNAR1 KO cells using CRISPR-Cas9 (Figure 6F; Figure S5F). Treatment of WT and IFNAR1 KO cells with IFN-α or IFN-β confirmed that the KO cells do not respond to extracellular IFNs (Figure 6G; Figure S5G). Similar to results obtained with the RLR and IRF3 KOs, inactivation of IFNAR1 signaling rescued cell viability associated with the loss of TDP-43 (Figures 6H and 6I; Figures S5H and S5I). Collectively, these results demonstrate that cell death associated with the loss of TDP-43 is mediated in a RLR- and IFNAR1-dependent manner.

IFNAR1 signaling promotes MLKL-dependent necroptosis

Type-I IFN-mediated cell death can occur through a variety of mechanisms. IFN-dependent necroptosis is one such pathway and is activated via IFNAR1 signaling and requires the serine/threonine-protein kinase 1/3 (RIPK1/3) and the necroptotic effector MLKL. Activated MLKL oligomerizes and forms cell-membrane pores to facilitate cell death (Thapa et al., 2013; Yang et al., 2020). We evaluated the expression of MLKL by western blot analysis of extracts from SH-SY5Y cells treated with either siCON or siTDP-43 and observed a striking increase in its levels in TDP-43-depleted cells (Figure 7A). MLKL is IFN inducible, and its overexpression has recently been observed to promote cell death (Arnež et al., 2015; Hildebrand et al., 2014; Knuth et al., 2019; Sarhan et al., 2019). Indeed, MLKL upregulation upon TDP-43 knockdown was only observed in WT and MDA5 KO cells, but not in the

MAVS KO, RIG-I KO, IFNAR1 KO, or IRF3-truncation cells (Figure 7B). These results were corroborated in the 786-O WT and KO cell lines (Figures S6A and S6B).

To determine whether MLKL overexpression is sufficient to promote cell death, we generated DOX-inducible FLAG-tagged MLKL SH-SY5Y and 786-O cell lines. DOX treatment induced FLAG-MLKL expression (Figures 7C; Figure S6C); 48 h after DOX treatment, we observed ~25%–40% reduced cell viability when compared with the no-DOX control (Figure 7D; Figure S6D). In addition, we observed ~50% reduction in ATP production by CellTiter Glo (Figure 7E; Figure S6E). Next, we generated MLKL KOs in SH-SY5Y and 786-O cells and quantified cell viability in siCON- and siTDP-43-treated cells (Figure 7F; Figure S6F). Although siTDP-43 resulted in an ~40% reduction in cell viability in WT cells, there was only an ~20% decrease in cell viability in MLKL KO cells (Figure 7G; Figure S6G). Moreover, MLKL KO significantly restored ATP production in cells treated with siTDP-43 (Figure 7H; Figure S6H). These results demonstrate that MLKL expression is IFN inducible and that its overexpression is sufficient to induce cell death in both SH-SY5Y and 786-O cells. Moreover, necroptosis contributes significantly to the mechanism behind cell death in TDP-43-deficient cells.

In summary, loss of TDP-43 results in the accumulation of immunostimulatory dsRNA, which activates RIG-I and culminates in IFN-mediated, necroptotic cell death.

DISCUSSION

Although best characterized in the context of host defense, RLRs are also important contributors to the efficacy of various anticancer approaches, and their inappropriate activation is associated with the development of autoimmunity (Heidegger et al., 2019; Jiang et al., 2019; Kato et al., 2017). Thus, the ability to control RLR activation is of importance across multiple facets of cellular and organismal homeostasis. TDP-43 is an essential RNA-binding protein implicated in the development of various pathologies, including ALS and FTLD (Mackenzie and Rademakers, 2008). Here, we demonstrate that loss of TDP-43 results in increased expression and mislocalization of several RNAPIII noncoding RNAs. Increased RNAPIII activity facilitates a RIG-Idependent IFN response that can be partially suppressed by overexpression of the cellular triphosphatase DUSP11, indicating the accumulated immunostimulatory dsRNAs are triphosphorylated. Moreover, RIG-I-dependent IFN-β production promotes MLKL-dependent necroptosis, which can be rescued via the genetic inactivation of the RLR pathway. Thus, our study uncovers an underappreciated and intricate relationship between the control of cellular gene expression and IFN-mediated cell death.

We have determined that TDP-43 regulates the accumulation of immunostimulatory dsRNA. Although we did not attempt to identify the J2$^+$ RNAs in SH-SY5Y cells, previous work in M17 neuroblastoma cells identified an enrichment of J2 binding in highly structured intronic regions of RNA as well as across the human endogenous retrovirus K (HERV-K) transcript in TDP43-depleted cells (Saldi et al., 2014). We anticipate that some of the J2$^+$ signal we observed is derived from RNAs previously identified. We have determined that J2$^+$ RNAs are immunostimulatory and that loss of TDP-43 potentiates a RIG-I-dependent IFN

response. RIG-I primarily discriminates RNA on the basis of a 5′-di or triphosphate structure at the end of RNAs, and thus, it is unlikely that J2-enriched HERV-K or intronic regions previously identified contribute significantly to RIG-I activation (Hornung et al., 2006; Pichlmair et al., 2006; Rehwinkel et al., 2010; Schlee et al., 2009; Schmidt et al., 2009). In support of post-mortem brain-tissue loss of TDP43 is associated with decondensation of intergenic chromatin (Liu et al., 2019). A reduction in H3K9me3, a repressive chromatin mark for repetitive elements, such as *Alus* and long interspersed elements (LINEs), was also observed. Interestingly, analysis of previously published TDP-43 iCLIP-sequencing data revealed that many of the upregulated RNAPIII transcripts are bound by TDP-43 (Tollervey et al., 2011). Moreover, we demonstrated that TDP-43 regulates the half-life of the RNAPIII transcript 7SL RNA and that this regulation requires the ability of TDP-43 to bind RNA. Although TDP-43 has been linked to the regulation of mRNA stability, our data further suggest that TDP-43 is involved in noncoding RNA decay (Tank et al., 2018). Whether this occurs co- or post-transcriptionally, that, the RIG-I-dependent IFN response is blunted by increasing the expression of the cellular RNA triphosphatase DUSP11.

We observed a significant remodeling of cellular gene expression in TDP-43-depleted cells. Among the most significant ontological terms associated with the upregulated genes were RNAPIII transcription. Indeed, by qRT-PCR, we confirmed the expression of many RNAPIII noncoding RNAs, including 7SL and *Alu* RNA, was significantly greater in cells lacking TDP-43. Increased RNAPIII-derived RNAs may stem from effects of TDP-43, either directly or indirectly, on chromatin modification and, therefore, RNAPIII transcription. For example, in human as well as which RNA decay machineries are involved, is unknown, and future studies will clarify this. Collectively, this suggests that increased RNAPIII transcripts in TDP-43-depleted cells result from a combination of alterations on transcription and RNA stability.

In TDP-43-depleted cells, we observed an increase in the cytoplasmic localization of several RNAPIII transcribed RNAs. Although 7SL RNA and *Alu* RNAs are normally cytoplasmic, the levels of the primarily nuclear 7SK snRNA were also increased in the cytoplasm. TDP-43 has been demonstrated to participate in the transport and localization of mRNPs in neuronal and dendritic cells; however, a role for it in 7SK snRNA localization has not been identified (Alami et al., 2014; Chou et al., 2018; Chu et al., 2019; Woerner et al., 2016). Additional studies are required to determine the mechanism by which TDP-43 influences 7SK snRNA expression and nuclear retention.

Regardless of the mechanism facilitating enhanced RNAPIII non-coding RNA expression, our work demonstrates that RNAPIII transcription is required for the IFN response in TDP43-depleted cells. Although RNAPIII has been identified as a cytoplasmic DNA sensor capable of activating RIG-I via the transcription of promoter-independent triphosphorylated RNAs, we do not anticipate this contributing too significantly to the cell-intrinsic immune response observed (Ablasser et al., 2009; Chiu et al., 2009). Rather, our data support a model in which RNAPIII-derived non-coding RNAs that can be bound by TDP43 are engaged by RIG-I to facilitate activation of MAVS and an IRF3-dependent IFN response. We speculate that the enhanced expression of RNAPIII transcripts results in a failure of their proper

processing and/or localization, which, in turn, facilities RIG-I activation. However, we cannot exclude the possibility that TDP-43 shields the select RNAPIII transcripts from RIG-I sensing. Indeed, the unshielding of 7SL RNA and RNA5SP141 transcripts because of the loss of their RBPs results in a RIG-I-dependent IFN response (Chiang et al., 2018; Nabet et al., 2017).

TDP-43 is associated with multiple neurological disorders, including ALS and FTLD. Interestingly, elevated IFN levels have been reported in the brains of patients with ALS and FTLD as well as in animal models (Hu et al., 2017; O'Rourke et al., 2016; Taylor et al., 2014; Wang et al., 2011). Multiple lines of evidence support a role for IFN signaling in neurodegeneration, including observations that high-dose IFN treatment can cause neurological abnormalities. Moreover, patients with Aicardi-Goutieres, an IFNopathy caused by mutations in MDA5, present with childhood neurodegeneration and dysfunction. Our demonstration that TDP-43 has a critical role in regulating immunostimulatory dsRNA accumulation suggests that activation of the RLR pathway may have a prominent role in initiating the neurological dysfunction observed in ALS and FTLD.

Our results here expand on an emerging theme in RLR activation: that host-encoded RNAs can be prominent RLR ligands and that cellular RBPs can function as cell-intrinsic checkpoints or barriers to RLR activation. Given these observations, we hypothesize that gene expression is inherently a dangerous process, not only in that alterations in gene expression programs can cause disease but also RNA structures involved in orchestrating the programs as well as the intermediates of RNA-processing reactions can be immunostimulatory. Moreover, this can be viewed as a proverbial double-edged sword because mechanisms that limit immunostimulatory dsRNAs may be pathogenic in the context of mutations but also leveraged therapeutically in conditions in which increased IFN signaling is desirable. Thus, we anticipate that continued investigations into mechanisms of gene expression will provide additional significant insight into the control of RLR activation by endogenous RNAs.

STAR★METHODS

RESOURCE AVAILABILITY

Lead contact—Further information and requests for reagents may be directed to, and will be fulfilled by the lead contact, John Karijolich.

Materials availability—All reagents generated in this study are available from the Lead Contact without restriction.

Date and code availability—The SH-SY5Y siCON/siTDP-43 RNA sequencing data have been deposited under accession number GEO: GSE162644.

EXPERIMENTAL MODEL AND SUBJECT DETAILS

Cell culture—786-O (ATCC), HEK293T (ATCC), and iSLK.BAC16 (Brulois et al., 2012) were maintained in Dulbecco's modified Eagle medium (DMEM; Invitrogen) supplemented with 10% fetal bovine serum (FBS; Invitrogen). SH-SY5Y (ATCC) were grown in 50:50

DMEM: Ham's F-12 nutrient mixture (Invitrogen) medium supplemented with 10% fetal bovine serum (FBS; Invitrogen). All cells were maintained with 100 U of penicillin/ml and 100 mg of streptomycin/ml (Invitrogen) at 37C under 5% CO_2.

METHOD DETAILS

Viruses—KSHV virions were isolated from iSLK.BAC16 cells that were reactivated with 1 µg/ml of doxycycline (Fisher Scientific) for 120 h by pelleting virus at 20,000 G for 2 h at 4C. KSHV virions were resuspended in PBS.

siRNA knockdown—SH-SY5Y and 786-O cells were transfected at 60%–80% confluency with 50 nM siRNA (sequences in Table S1) or MISSION siRNA Universal Negative Control #1 (Sigma) using Lipofectamine RNAiMax (Invitrogen). 48 h post-transfection cells were collected.

Immunofluorescence microscopy—SH-SY5Y cells, cultured on poly-L-lysine treated glass coverslip, were transfected at 60%–80% confluency with siRNAs for 48 h. Cells were fixed in 4% paraformaldehyde, permeabilized in 0.25% Triton-X, blocked in blocking buffer (3% BSA, 5% Normal Goat Serum (Thermo), 0.1% Tween) and incubated in primary antibody (TDP-43: 1:400; J2: 1:100). Slides were incubated with Rhodamine red anti-mouse and Cyanine 5 anti-rabbit secondary antibodies (Thermo Scientific; diluted 1:750) and were mounted in mounting media (Thermo). Cells were imaged with an Olympus FV1000 confocal microscope.

J2 immunoprecipitation (IP)—SH-SY5Y cells were transfected with siRNAs for 48 h. Cells were washed in PBS and RNA was isolated by TRIzol (Invitrogen) in accordance with the manufacturer's instructions. RNA was DNase I (NEB) treated at 37°C for 20 minutes and inactivated with EDTA at 70°C for 10 minutes followed by phenol chloroform extraction. 15 µg of RNA was incubated with 2 µg of J2 antibody (Scicons) or control IgG (Cell Signaling) in binding buffer (50 mM Tris [pH 8.0], 150 mM NaCl, 1mM EDTA, 1% NP-40, 5mM MgCl2) with Ribo-lock (Thermo) at 4°C overnight. IPs were incubated with SureBeads Protein G magnetic beads (Bio-rad) at 4°C for 4 h, washed five times in binding buffer, and RNA was eluted in TRIzol. J2-isolated RNA was either Mock or CIAP (Promega)-treated at 37°C for 1 h, followed by PCA extraction. 100 ng of RNA was transfected into 786-O cells at 60%–80% confluency with Lipofectamine RNAiMax. 24 h post-transfection cells were collected and analyzed by RT-qPCR.

Nucleic acid isolation and measurement—For analysis of gene expression by RT-qPCR, total RNA was isolated with TRIzol (Invitrogen) in accordance with the manufacturer's instructions. RNA was DNase I (NEB) treated at 37°C for 20 minutes and inactivated with EDTA at 70°C for 10 minutes. cDNA was synthesized from DNase-treated RNA with random 9-mer (Integrated DNA Technologies) and M-MLV RT (Promega). qPCR was performed using the PowerUp SYBR Green qPCR kit (Thermo Scientific) with appropriate primers (Table S1).

Subcellular fractionation and western blotting—Subcellular fractionation was performed using the REAP method with the minor modification of using one 10-cm plate for each fractionation condition (Suzuki et al., 2010).

Cell lysates were prepared with lysis buffer (50 mM Tris [pH 7.6], 150 mM NaCl, 0.5% NP-40) and quantified by Bradford assay. Equivalent amounts of each sample were resolved by SDS-PAGE, electrotransferred to PVDF membrane, and blotted for the indicated proteins (Table S1). Primary antibodies were followed by AlexaFluor 680-or −800 conjugated anti-rabbit and anti-mouse secondary antibodies (Life Technologies; 1:5000) and visualized by Li-Cor Odyssey.

KSHV infection—SH-SY5Y and 786-O cells were treated with siRNA for 48 h prior to infection. KSHV virions were added to the media and supplemented with 2% polyethylene glycol (PEG(VWR)) and 8 μg/ml of polybrene (Sigma). Cells were spun at 1,000 rpm for 30 min at room temperature. Fresh media was then added, and the cells were incubated for 24 h, followed by analysis by RT-qPCR.

CRISPR/Cas9 cloning, lentiviral production, and infection—Single-guide RNAs (sgRNAs) (sequences in Table S1) were selected by inputting gene sequences into the Broad Institute GPP sgRNA CRISPR KO Designer. Two high-score sgRNAs were selected for each gene. sgRNA oligos were cloned into the lentiCRISPR V2 (Addgene) lentiviral plasmid according to depositor instructions.

Lentivirus was prepared in HEK293T cells. Cells were transfected at 50%–60% confluency with lentiCRISPR V2, psPAX2 (lentiviral packaging), and pMD2.G (lentiviral envelope) (Addgene) using polyjet (SignaGen). 72 h post-transfection the supernatant was collected, mixed with 8 μg/ml of polybrene and 1% PEG, and added to SH-SY5Y, 786-O, or HEK293T cells that were spinfected at 1,000 rpm for 1 h at room temperature. Cells were selected for 2 weeks in media containing either 300 μg/ml hygromycin B (Invitrogen; rtTA doxycycline-inducible element), 5 μg/ml blasticidin (Invivogen; inducible RIG-I), or 5 μg/ml puromycin (Sigma; lenti-CRISPR V2 knockouts).

Knockout generation—Cells were infected with lentivirus. Following puromycin selection, single cell clones were grown out in 48-well plates. The knockout was verified by western blot of the respective protein. CRISPR/Cas9 induced mutations were identified by isolation of genomic DNA (Promega), PCR of the genomic region where the guide RNA targets, TOPO cloning, and Sanger sequencing of the PCR product (Mutations listed in Table S2). For select knockouts, 100 ng/ml of the RIG-I ligand 3p-hpRNA (Invivogen) was transfected into cells for 6 h, followed by RNA isolation and RT-qPCR. For IFNAR1 knockouts, recombinant IFN a and b were added to cells for 8 h, followed by RNA isolation and RT-qPCR.

Cloning and cell line generation—RIG-I pLenti-CMVtight-FL-HA-DEST-Blast (Zhao et al., 2018) underwent site-directed mutagenesis (SDM) to mutate the RIG-I sgRNA recognition sequence to prevent CRISPR/Cas9 cleavage. Lentivirus was produced and used to transduce SH-SY5Y and 786-O RIG-I knockout cells followed by antibiotic selection.

Cells were then transduced with lentiviral particles produced from pLenti CMV rtTA3 Hygro (Addgene) to create a Tet-On inducible system, followed by antibiotic selection.

DUSP11 was PCR amplified from SH-SY5Y mRNA and Gateway cloned into the pLenti-CMV-tight-blast-dest vector. MLKL was PCR amplified from MLKL pF-TRE3G-PGK-puro (generously provided by Dr. James Murphy [Petrie et al., 2018]) and Gateway cloned into pLenti-CMV-tight-blast-dest vector. HEK293T, 786-O, and SH-SY5Y cells were transduced with lentiviral particles produced from pLenti CMV rtTA3 Hygro (Addgene) to create a Tet-On inducible system, followed by antibiotic selection. RIG-I, DUSP11, and MLKL lentivirus was then produced and used to transduce either HEK293T rtTA3 cells (RIG-I), or 786-O and SH-SY5Y rtTA3 cells (DUSP11, MLKL) followed by antibiotic selection. FLAG-TDP-43 pcDNA3 WT and mutRRM (with W113A/R151A mutations) plasmids were generously provided by Dr. J. Paul Taylor (Freibaum et al., 2010).

RNA sequencing—SH-SY5Y RIG-I complement cells were treated with siRNA for 48 h. Doxycycline was added to induce RIG-I expression for the final 24 h. Total RNA was isolated using TRIzol, DNase treated, and rRNA depleted (NEB). RNA sequencing libraries were generated using the Collibri Stranded RNA library prep kit (Thermo) according to the manufacture recommendations. Libraries were then subjected to paired-end sequencing on a NovaSeq 6000 at the Vanderbilt Technologies for Advanced Genomics (VANTAGE). Data are submitted in SRA and will be available upon publication.

RNA sequencing data analysis—Raw read quality was assessed using FastQC (v0.11.5). STAR (v2.7.3a) was used to align reads to the human genome (GRCh38). The transcript quantification was done using featureCounts using the pair-end mode to count both reads that uniquely mapped. Differentially expressed genes were called using edgeR (v2.26.5) with Benjamini-Hochberg adjusted p value < 0.01 and log2FoldChange > 2. R package clusterProfiler (v3.12.0) was used for the gene set over-representation analysis with the KEGG database. K-means clustering was applied to gene expression values (normalized by count per million) using R function kmeans (from R package stats) and the number of clusters was determined by total within sum of square. Heatmaps were generated using pheatmap (v1.0.12). For making IGV figures, the bam files were first transformed into bigwig file with a bin size of 10bp and normalized by CPM (count per million). Then the bigwig files were loaded into IGV viewer to view the read distribution on target genes.

Northern blot—SH-SY5Y RIG-I complement cells were treated with siRNA for 48 h. Doxycycline was added to induce RIG-I expression for the final 24 h. Total RNA was isolated using TRIzol followed by 1h DNase treatment and PCA extraction. 25 μg of RNA was mixed with loading buffer (Formamide, bromophenol blue, xylene cyanol, EDTA), denatured at 90°C for 2min, loaded on a 10% TBE-urea gel, and run at 20W for ~2 h. RNA was transferred onto nylon membrane in TBE buffer at 4°C overnight followed by twice crosslinking at 254 nm. The membrane was incubated with the hybridization buffer (1M sodium phosphate [pH 6.5], 20X SSC, 50X Denhardts, 20% SDS) at 42°C for 1h, replaced with fresh hybridization buffer, and supplemented with 10% PEG. Labeled probes were added to the buffer and incubated at 42°C overnight. The membrane was washed 3X in wash

buffer (0.5X SSC, 0.1%SDS) followed by exposure on a film. The film was developed on the Typhoon FLA 7000 (GE Healthcare).

Endogenous TDP-43 immunoprecipitation—SH-SY5Y cells were washed twice in cold PBS, crosslinked with 0.5% formaldehyde for 10 min in PBS, quenched with 0.3M glycine for 5min, and washed twice with cold PBS. Cells were resuspended in RIP buffer (150 mM KCl, 25mM Tris [pH 7.4], 5mM EDTA, 0.5mM DTT, 0.5% NP-40) and kept on ice for 20min followed by sonication. Protein G beads (Biorad) were washed in RIP buffer, followed by the addition of 2.5 mg of IgG (Thermo) or TDP-43 antibody (Proteintech) and incubated at room temp for 30min. Excess antibody was removed. Soluble cell extract was added to bead-antibody complex and incubated at 4°C for 3 h. Beads were washed three times for 10 min with RIP buffer followed by DNase treatment. Protein-RNA crosslinks were reversed by adding reverse crosslink buffer (100 mM Tris [pH 8], 10mM EDTA, 1% SDS, 0.5% DTT) to samples and heated at 70°C for 45 min. RNA was recovered by TRIzol extraction followed by isopropanol precipitation and RT-qPCR analysis. Protein was recovered in 300mM glycine [pH 2.5] at RT for 15 min and analyzed by western blot.

RIG-I RNA immunoprecipitation—SH-SY5Y RIG-I complement cells were treated with siRNA for 48 h. Doxycycline was added to induce RIG-I expression for the final 24 h. Cells were washed twice in cold PBS, crosslinked with 0.5% formaldehyde for 10 min in PBS, quenched with 0.3M glycine for 5min, and washed twice with cold PBS. Cells were resuspended in RIPA buffer (50mM Tris [pH 8.0], 0.5% sodium deoxycholate, 0.05% SDS, 1mM EDTA, 150mM NaCl, 1mM DTT, 1% NP-40) and kept on ice for 20min followed by sonication. Anti-Flag M2 magnetic resin (Sigma) was washed in RIPA buffer followed by the addition of soluble extract and incubation at 4°C for 3 h. Beads were washed three times for 10 min at 4°C and then two times for 5 min at room temperature in RIPA buffer with 0.1%SDS, 1M NaCl, and 1M urea. Resin was eluted with 1X FLAG peptide (Sigma) in RIPA buffer for 45 min at 4°C. Crosslinks were reversed by adding 100 mM Tris [pH 8], 10mM EDTA, 1% SDS and 2% DTT to samples and heated at 70°C for 45 min. RNA was recovered by TRIzol extraction, isopropanol precipitation, DNase treatment, PCA extraction, and ethanol precipitation. Bound RNAs were analyzed by RT-qPCR.

Cell viability assays—SH-SY5Y and 786-O cells were treated with siRNAs for 120 h and 96 h, respectively. Trypan Blue: Cells were trypsinized (GIBCO) and diluted 1:1 with trypan blue stain. The mixture was incubated for 1 min, followed by counting by Cell Countess II. CellTiter-Glo: Cells were equilibrated at room temperature for ~30 min. An equal volume of CellTiter-Glo reagent (Promega) was added to wells, mixed and lysed for 2 min, incubated for 10 min, and luminescence was read.

Small molecular inhibitor treatment—Cells were treated with 100 mM RNAPIII inhibitor CAS 577784–91-9 (Millipore) or vehicle at the same time as siRNA treatment. Cells were collected 24 h post transfection followed by RT-qPCR analysis.

RNA decay—SH-SY5Y: Cells were transfected with siCON/siTDP-43 for 48h. 100 mM RNAPIII inhibitor was added after 48h and cells were collected at indicated time points. RNA was isolated and followed by RT-qPCR analysis. HEK293T TDP-43 KO: Cells were

transfected with pcDNA3, WT TDP-43, or TDP-43 RRM for 24h. 100 mM RNAPIII inhibitor was added and cells were collected at indicated time points. RNA was isolated and followed by RT-qPCR analysis.

QUANTIFICATION AND STATISTICAL ANALYSIS

Statistical parameters are reported in the figures and corresponding figure legends. Student t test was used to determine statistical significance * p   0.05; ** p   0.005; *** p   0.0005; ns: not significant. The results were expressed as mean ± SD. Value of n is depicted in each figure legend. Confocal microscopy was performed on the Olympus FV-100 (Olympus) microscope and the scale bar on the images is 20um. qPCR was performed using the QuantStudio 3 (Thermo). Immunoblots were developed using the Odyssey Li-Cor (Li-Cor). RNA sequencing was performed using the NovaSeq 6000 (Illumina). Northern blot was analyzed by Typhoon FLA 7000 (GE Healthcare) and signal intensities were quantified using ImageJ software. Cell death was analyzed by Countess II (Thermo) and luminomenter (Promega).

Supplementary Material

Refer to Web version on PubMed Central for supplementary material.

ACKNOWLEDGMENTS

REFERENCES

Ablasser A, Bauernfeind F, Hartmann G, Latz E, Fitzgerald KA, and Hornung V (2009). RIG-I-dependent sensing of poly(dA:dT) through the induction of an RNA polymerase III-transcribed RNA intermediate. Nat. Immunol 10, 1065–1072. [PubMed: 19609254]

Alami NH, Smith RB, Carrasco MA, Williams LA, Winborn CS, Han SSW, Kiskinis E, Winborn B, Freibaum BD, Kanagaraj A, et al. (2014). Axonal transport of TDP-43 mRNA granules is impaired by ALS-causing mutations. Neuron 81, 536–543. [PubMed: 24507191]

Arnez KH, Kindlova M, Bokil NJ, Murphy JM, Sweet MJ, and Guncar G (2015). Analysis of the N-terminal region of human MLKL, as well as two distinct MLKL isoforms, reveals new insights into necroptotic cell death. Biosci. Rep 36, e00291. [PubMed: 26704887]

Biacchesi S, LeBerre M, Lamoureux A, Louise Y, Lauret E, Boudinot P, and Brémont M (2009). Mitochondrial antiviral signaling protein plays a major role in induction of the fish innate immune response against RNA and DNA viruses. J. Virol 83, 7815–7827. [PubMed: 19474100]

Bose JK, Huang C-C, and Shen C-KJ (2011). Regulation of autophagy by neuropathological protein TDP-43. J. Biol. Chem 286, 44441–44448. [PubMed: 22052911]

Bou-Nader C, Gordon JM, Henderson FE, and Zhang J (2019). The search for a PKR code-differential regulation of protein kinase R activity by diverse RNA and protein regulators. RNA 25, 539–556. [PubMed: 30770398]

Brulois KF, Chang H, Lee AS-Y, Ensser A, Wong L-Y, Toth Z, Lee SH, Lee H-R, Myoung J, Ganem D, et al. (2012). Construction and manipulation of a new Kaposi's sarcoma-associated herpesvirus bacterial artificial chromosome clone. J. Virol 86, 9708–9720. [PubMed: 22740391]

Buratti E, and Baralle FE (2012). TDP-43: gumming up neurons through protein-protein and protein-RNA interactions. Trends Biochem. Sci 37, 237–247. [PubMed: 22534659]

Burke JM, and Sullivan CS (2017). DUSP11—an RNA phosphatase that regulates host and viral non-coding RNAs in mammalian cells. RNA Biol. 14, 1457–1465. [PubMed: 28296624]

Burke JM, Kincaid RP, Nottingham RM, Lambowitz AM, and Sullivan CS (2016). DUSP11 activity on triphosphorylated transcripts promotes Argonaute association with noncanonical viral microRNAs and regulates steadystate levels of cellular noncoding RNAs. Genes Dev. 30, 2076–2092. [PubMed: 27798849]

Chen YG, Kim MV, Chen X, Batista PJ, Aoyama S, Wilusz JE, Iwasaki A, and Chang HY (2017). Sensing Self and Foreign Circular RNAs by Intron Identity. Mol. Cell 67, 228–238.e5. [PubMed: 28625551]

Chiang JJ, Sparrer KMJ, van Gent M, Lässig C, Huang T, Osterrieder N, Hopfner K-P, and Gack MU (2018). Viral unmasking of cellular 5S rRNA pseudogene transcripts induces RIG-I-mediated immunity. Nat. Immunol 19, 53–62. [PubMed: 29180807]

Chiu Y-H, Macmillan JB, and Chen ZJ (2009). RNA polymerase III detects cytosolic DNA and induces type I interferons through the RIG-I pathway. Cell 138, 576–591. [PubMed: 19631370]

Choi UY, Kang J-S, Hwang YS, and Kim Y-J (2015). Oligoadenylate synthase-like (OASL) proteins: dual functions and associations with diseases. Exp. Mol. Med 47, e144. [PubMed: 25744296]

Chou C-C, Zhang Y, Umoh ME, Vaughan SW, Lorenzini I, Liu F, Sayegh M, Donlin-Asp PG, Chen YH, Duong DM, et al. (2018). TDP43 pathology disrupts nuclear pore complexes and nucleocytoplasmic transport in ALS/FTD. Nat. Neurosci 21, 228–239. [PubMed: 29311743]

Chu J-F, Majumder P, Chatterjee B, Huang S-L, and Shen CJ (2019). TDP-43 Regulates Coupled Dendritic mRNA Transport-Translation Processes in Co-operation with FMRP and Staufen1. Cell Rep. 29, 3118–3133.e6. [PubMed: 31801077]

Chung C-Y, Berson A, Kennerdell JR, Sartoris A, Unger T, Porta S, Kim H-J, Smith ER, Shilatifard A, Van Deerlin V, et al. (2018). Aberrant activation of non-coding RNA targets of transcriptional elongation complexes contributes to TDP-43 toxicity. Nat. Commun 9, 4406. [PubMed: 30353006]

Freibaum BD, Chitta RK, High AA, and Taylor JP (2010). Global analysis of TDP-43 interacting proteins reveals strong association with RNA splicing and translation machinery. J. Proteome Res 9, 1104–1120. [PubMed: 20020773]

Giffin L, and Damania B (2014). KSHV: pathways to tumorigenesis and persistent infection. Adv. Virus Res 88, 111–159. [PubMed: 24373311]

Heidegger S, Wintges A, Stritzke F, Bek S, Steiger K, Koenig P-A, Göttert S, Engleitner T, Öllinger R, Nedelko T, et al. (2019). RIG-I activation is critical for responsiveness to checkpoint blockade. Sci. Immunol 4, eaau8943. [PubMed: 31519811]

Hildebrand JM, Tanzer MC, Lucet IS, Young SN, Spall SK, Sharma P, Pierotti C, Garnier J-M, Dobson RCJ, Webb AI, et al. (2014). Activation of the pseudokinase MLKL unleashes the four-helix bundle domain to induce membrane localization and necroptotic cell death. Proc. Natl. Acad. Sci. USA 111, 15072–15077. [PubMed: 25288762]

Hornung V, Ellegast J, Kim S, Brzózka K, Jung A, Kato H, Poeck H, Akira S, Conzelmann K-K, Schlee M, et al. (2006). 5′-Triphosphate RNA is the ligand for RIG-I. Science 314, 994–997. [PubMed: 17038590]

Hou F, Sun L, Zheng H, Skaug B, Jiang Q-X, and Chen ZJ (2011). MAVS forms functional prion-like aggregates to activate and propagate antiviral innate immune response. Cell 146, 448–461. [PubMed: 21782231]

Hu Y, Cao C, Qin X-Y, Yu Y, Yuan J, Zhao Y, and Cheng Y (2017). Increased peripheral blood inflammatory cytokine levels in amyotrophic lateral sclerosis: a meta-analysis study. Sci. Rep 7, 9094. [PubMed: 28831083]

Iguchi Y, Katsuno M, Niwa JI, Yamada SI, Sone J, Waza M, Adachi H, Tanaka F, Nagata KI, Arimura N, et al. (2009). TDP-43 depletion induces neuronal cell damage through dysregulation of Rho family GTPases. J. Biol. Chem. 284, 22059–22066. [PubMed: 19535326]

Jiang X, Muthusamy V, Fedorova O, Kong Y, Kim DJ, Bosenberg M, Pyle AM, and Iwasaki A (2019). Intratumoral delivery of RIG-I agonist SLR14 induces robust antitumor responses. J. Exp. Med 216, 2854–2868. [PubMed: 31601678]

Kato H, Takeuchi O, Sato S, Yoneyama M, Yamamoto M, Matsui K, Uematsu S, Jung A, Kawai T, Ishii KJ, et al. (2006). Differential roles of MDA5 and RIG-I helicases in the recognition of RNA viruses. Nature 441, 101–105. [PubMed: 16625202]

Kato H, Takeuchi O, Mikamo-Satoh E, Hirai R, Kawai T, Matsushita K, Hiiragi A, Dermody TS, Fujita T, and Akira S (2008). Length-dependent recognition of double-stranded ribonucleic acids by retinoic acid-inducible gene-I and melanoma differentiation-associated gene 5. J. Exp. Med 205, 1601–1610. [PubMed: 18591409]

Kato H, Oh S-W, and Fujita T (2017). RIG-I-like receptors and type I interferonopathies. J. Interferon Cytokine Res 37, 207–213. [PubMed: 28475461]

Kawahara Y, and Mieda-Sato A (2012). TDP-43 promotes microRNA biogenesis as a component of the Drosha and Dicer complexes. Proc. Natl. Acad. Sci. USA 109, 3347–3352. [PubMed: 22323604]

Kawasaki T, and Kawai T (2014). Toll-like receptor signaling pathways. Front. Immunol 5, 461. [PubMed: 25309543]

Kim U, Wang Y, Sanford T, Zeng Y, and Nishikura K (1994). Molecular cloning of cDNA for double-stranded RNA adenosine deaminase, a candidate enzyme for nuclear RNA editing. Proc. Natl. Acad. Sci. USA 91, 11457–11461. [PubMed: 7972084]

Knuth A-K, Rösler S, Schenk B, Kowald L, van Wijk SJL, and Fulda S (2019). Interferons Transcriptionally up-regulate MLKL expression in cancer cells. Neoplasia 21, 74–81. [PubMed: 30521981]

König J, Zarnack K, Rot G, Curk T, Kayikci M, Zupan B, Turner DJ, Luscombe NM, and Ule J (2010). iCLIP reveals the function of hnRNP particles in splicing at individual nucleotide resolution. Nat. Struct. Mol. Biol 17, 909–915. [PubMed: 20601959]

Kraemer BC, Schuck T, Wheeler JM, Robinson LC, Trojanowski JQ, Lee VMY, and Schellenberg GD (2010). Loss of murine TDP-43 disrupts motor function and plays an essential role in embryogenesis. Acta Neuropathol. 119, 409–419. [PubMed: 20198480]

Lalmansingh AS, Urekar CJ, and Reddi PP (2011). TDP-43 is a transcriptional repressor: the testis-specific mouse acrv1 gene is a TDP-43 target in vivo. J. Biol. Chem 286, 10970–10982. [PubMed: 21252238]

Liddicoat BJ, Piskol R, Chalk AM, Ramaswami G, Higuchi M, Hartner JC, Li JB, Seeburg PH, and Walkley CR (2015). RNA editing by ADAR1 prevents MDA5 sensing of endogenous dsRNA as nonself. Science 349, 1115–1120. [PubMed: 26275108]

Liu EY, Russ J, Cali CP, Phan JM, Amlie-Wolf A, and Lee EB (2019). Loss of nuclear TDP-43 is associated with decondensation of LINE retrotransposons. Cell Rep. 27, 1409–1421.e6. [PubMed: 31042469]

Loo Y-M, and Gale M Jr. (2011). Immune signaling by RIG-I-like receptors. Immunity 34, 680–692. [PubMed: 21616437]

Mackenzie IRA, and Rademakers R (2008). The role of TDP-43 in amyotrophic lateral sclerosis and frontotemporal dementia. Curr. Opin. Neurol 21, 693–700. [PubMed: 18989115]

Mannion NM, Greenwood SM, Young R, Cox S, Brindle J, Read D, Nellåker C, Vesely C, Ponting CP, McLaughlin PJ, et al. (2014). The RNA-editing enzyme ADAR1 controls innate immune responses to RNA. Cell Rep. 9, 1482–1494. [PubMed: 25456137]

Melcher T, Maas S, Herb A, Sprengel R, Seeburg PH, and Higuchi M (1996). A mammalian RNA editing enzyme. Nature 379, 460–464. [PubMed: 8559253]

Mitra J, Guerrero EN, Hegde PM, Liachko NF, Wang H, Vasquez V, Gao J, Pandey A, Taylor JP, Kraemer BC, et al. (2019). Motor neuron disease-associated loss of nuclear TDP-43 is linked to DNA double-strand break repair defects. Proc. Natl. Acad. Sci. USA 116, 4696–4705. [PubMed: 30770445]

Nabet BY, Qiu Y, Shabason JE, Wu TJ, Yoon T, Kim BC, Benci JL, DeMichele AM, Tchou J, Marcotrigiano J, and Minn AJ (2017). Exosome RNA unshielding couples stromal activation to pattern recognition receptor signaling in cancer. Cell 170, 352–366.e13. [PubMed: 28709002]

Nishikura K, Yoo C, Kim U, Murray JM, Estes PA, Cash FE, and Liebhaber SA (1991). Substrate specificity of the dsRNA unwinding/modifying activity. EMBO J. 10, 3523–3532. [PubMed: 1915306]

O'Rourke JG, Bogdanik L, Yáñez A, Lall D, Wolf AJ, Muhammad AKMG, Ho R, Carmona S, Vit JP, Zarrow J, et al. (2016). C9orf72 is required for proper macrophage and microglial function in mice. Science 351, 1324–1329. [PubMed: 26989253]

Pestal K, Funk CC, Snyder JM, Price ND, Treuting PM, and Stetson DB (2015). Isoforms of RNA-editing enzyme ADAR1 independently control nucleic acid sensor MDA5-driven autoimmunity and multi-organ development. Immunity 43, 933–944. [PubMed: 26588779]

Petrie EJ, Sandow JJ, Jacobsen AV, Smith BJ, Griffin MDW, Lucet IS, Dai W, Young SN, Tanzer MC, Wardak A, et al. (2018). Conformational switching of the pseudokinase domain promotes human MLKL tetramerization and cell death by necroptosis. Nat. Commun 9, 2422. [PubMed: 29930286]

Pichlmair A, Schulz O, Tan CP, Näslund TI, Liljeström P, Weber F, and Reis e Sousa C (2006). RIG-I-mediated antiviral responses to single-stranded RNA bearing 5′-phosphates. Science 314, 997–1001. [PubMed: 17038589]

Polymenidou M, Lagier-Tourenne C, Hutt KR, Huelga SC, Moran J, Liang TY, Ling S-C, Sun E, Wancewicz E, Mazur C, et al. (2011). Long pre-mRNA depletion and RNA missplicing contribute to neuronal vulnerability from loss of TDP-43. Nat. Neurosci 14, 459–468. [PubMed: 21358643]

Prasad A, Bharathi V, Sivalingam V, Girdhar A, and Patel BK (2019). Molecular mechanisms of TDP-43 misfolding and pathology in amyotrophic lateral sclerosis. Front. Mol. Neurosci 12, 25. [PubMed: 30837838]

Rehwinkel J, Tan CP, Goubau D, Schulz O, Pichlmair A, Bier K, Robb N, Vreede F, Barclay W, Fodor E, and Reis e Sousa C (2010). RIG-I detects viral genomic RNA during negative-strand RNA virus infection. Cell 140, 397–408. [PubMed: 20144762]

Reikine S, Nguyen JB, and Modis Y (2014). Pattern recognition and signaling mechanisms of RIG-I and MDA5. Front. Immunol 5, 342. [PubMed: 25101084]

Saldi TK, Ash PE, Wilson G, Gonzales P, Garrido-Lecca A, Roberts CM, Dostal V, Gendron TF, Stein LD, Blumenthal T, et al. (2014). TDP-1, the Caenorhabditis elegans ortholog of TDP-43, limits the accumulation of double-stranded RNA. EMBO J. 33, 2947–2966. [PubMed: 25391662]

Sarhan J, Liu BC, Muendlein HI, Weindel CG, Smirnova I, Tang AY, Ilyukha V, Sorokin M, Buzdin A, Fitzgerald KA, and Poltorak A (2019). Constitutive interferon signaling maintains critical threshold of MLKL expression to license necroptosis. Cell Death Differ. 26, 332–347. [PubMed: 29786074]

Schlee M, Roth A, Hornung V, Hagmann CA, Wimmenauer V, Barchet W, Coch C, Janke M, Mihailovic A, Wardle G, et al. (2009). Recognition of 5′- triphosphate by RIG-I helicase requires short blunt double-stranded RNA as contained in panhandle of negative-strand virus. Immunity 31, 25–34. [PubMed: 19576794]

Schmid B, Hruscha A, Hogl S, Banzhaf-Strathmann J, Strecker K, van der Zee J, Teucke M, Eimer S, Hegermann J, Kittelmann M, et al. (2013). Loss of ALS-associated TDP-43 in zebrafish causes muscle degeneration, vascular dysfunction, and reduced motor neuron axon outgrowth. Proc. Natl. Acad. Sci. USA 110, 4986–4991. [PubMed: 23457265]

Schmidt A, Schwerd T, Hamm W, Hellmuth JC, Cui S, Wenzel M, Hoffmann FS, Michallet M-C, Besch R, Hopfner K-P, et al. (2009). 5′-triphosphate RNA requires base-paired structures to activate antiviral signaling via RIG-I. Proc. Natl. Acad. Sci. USA 106, 12067–12072. [PubMed: 19574455]

Shelkovnikova TA, Kukharsky MS, An H, Dimasi P, Alexeeva S, Shabir O, Heath PR, and Buchman VL (2018). Protective paraspeckle hyper-assembly downstream of TDP-43 loss of function in amyotrophic lateral sclerosis. Mol. Neurodegener 13, 30. [PubMed: 29859124]

Suzuki K, Bose P, Leong-Quong RY, Fujita DJ, and Riabowol K (2010). REAP: a two minute cell fractionation method. BMC Res. Notes 3, 294. [PubMed: 21067583]

Tank EM, Figueroa-Romero C, Hinder LM, Bedi K, Archbold HC, Li X, Weskamp K, Safren N, Paez-Colasante X, Pacut C, et al. (2018). Abnormal RNA stability in amyotrophic lateral sclerosis. Nat. Commun 9, 2845. [PubMed: 30030424]

Taylor JM, Minter MR, Newman AG, Zhang M, Adlard PA, and Crack PJ (2014). Type-1 interferon signaling mediates neuro-inflammatory events in models of Alzheimer's disease. Neurobiol. Aging 35, 1012–1023. [PubMed: 24262201]

Thapa RJ, Nogusa S, Chen P, Maki JL, Lerro A, Andrake M, Rall GF, Degterev A, and Balachandran S (2013). Interferon-induced RIP1/RIP3mediated necrosis requires PKR and is licensed by FADD and caspases. Proc. Natl. Acad. Sci. USA 110, E3109–E3118. [PubMed: 23898178]

Tollervey JR, Curk T, Rogelj B, Briese M, Cereda M, Kayikci M, König J, Hortobágyi T, Nishimura AL, Zupunski V, et al. (2011). Characterizing the RNA targets and position-dependent splicing regulation by TDP-43. Nat. Neurosci 14, 452–458. [PubMed: 21358640]

Vanden Broeck L, Callaerts P, and Dermaut B (2014). TDP-43-mediated neurodegeneration: towards a loss-of-function hypothesis? Trends Mol. Med 20, 66–71. [PubMed: 24355761]

Wang R, Yang B, and Zhang D (2011). Activation of interferon signaling pathways in spinal cord astrocytes from an ALS mouse model. Glia 59, 946–958. [PubMed: 21446050]

Weber F, Wagner V, Rasmussen SB, Hartmann R, and Paludan SR (2006). Double-stranded RNA is produced by positive-strand RNA viruses and DNA viruses but not in detectable amounts by negative-strand RNA viruses. J. Virol 80, 5059–5064. [PubMed: 16641297]

White RJ (2011). Transcription by RNA polymerase III: more complex than we thought. Nat. Rev. Genet 12, 459–463. [PubMed: 21540878]

Woerner AC, Frottin F, Hornburg D, Feng LR, Meissner F, Patra M, Tatzelt J, Mann M, Winklhofer KF, Hartl FU, and Hipp MS (2016). Cytoplasmic protein aggregates interfere with nucleocytoplasmic transport of protein and RNA. Science 351, 173–176. [PubMed: 26634439]

Wu Y, Zhao W, Liu Y, Tan X, Li X, Zou Q, Xiao Z, Xu H, Wang Y, and Yang X (2018). Function of HNRNPC in breast cancer cells by controlling the dsRNA-induced interferon response. EMBO J. 37, e99017. [PubMed: 30158112]

Yang D, Liang Y, Zhao S, Ding Y, Zhuang Q, Shi Q, Ai T, Wu S-Q, and Han J (2020). ZBP1 mediates interferon-induced necroptosis. Cell. Mol. Immunol 17, 356–368. [PubMed: 31076724]

Zarnack K, König J, Tajnik M, Martincorena I, Eustermann S, Stévant I, Reyes A, Anders S, Luscombe NM, and Ule J (2013). Direct competition between hnRNP C and U2AF65 protects the transcriptome from the exonization of Alu elements. Cell 152, 453–466. [PubMed: 23374342]

Zhao Y, Ye X, Dunker W, Song Y, and Karijolich J (2018). RIG-I like receptor sensing of host RNAs facilitates the cell-intrinsic immune response to KSHV infection. Nat. Commun 9, 4841. [PubMed: 30451863]

Highlights

- Loss of TDP-43 causes accumulation of immunostimulatory double-stranded RNA (dsRNA)

- Immunostimulatory dsRNA comprises RNA polymerase III transcripts

- Immunostimulatory dsRNA is detected by RIG-I

- Lethality of TDP-43 can be rescued by genetic inactivation of the RIG-I pathway
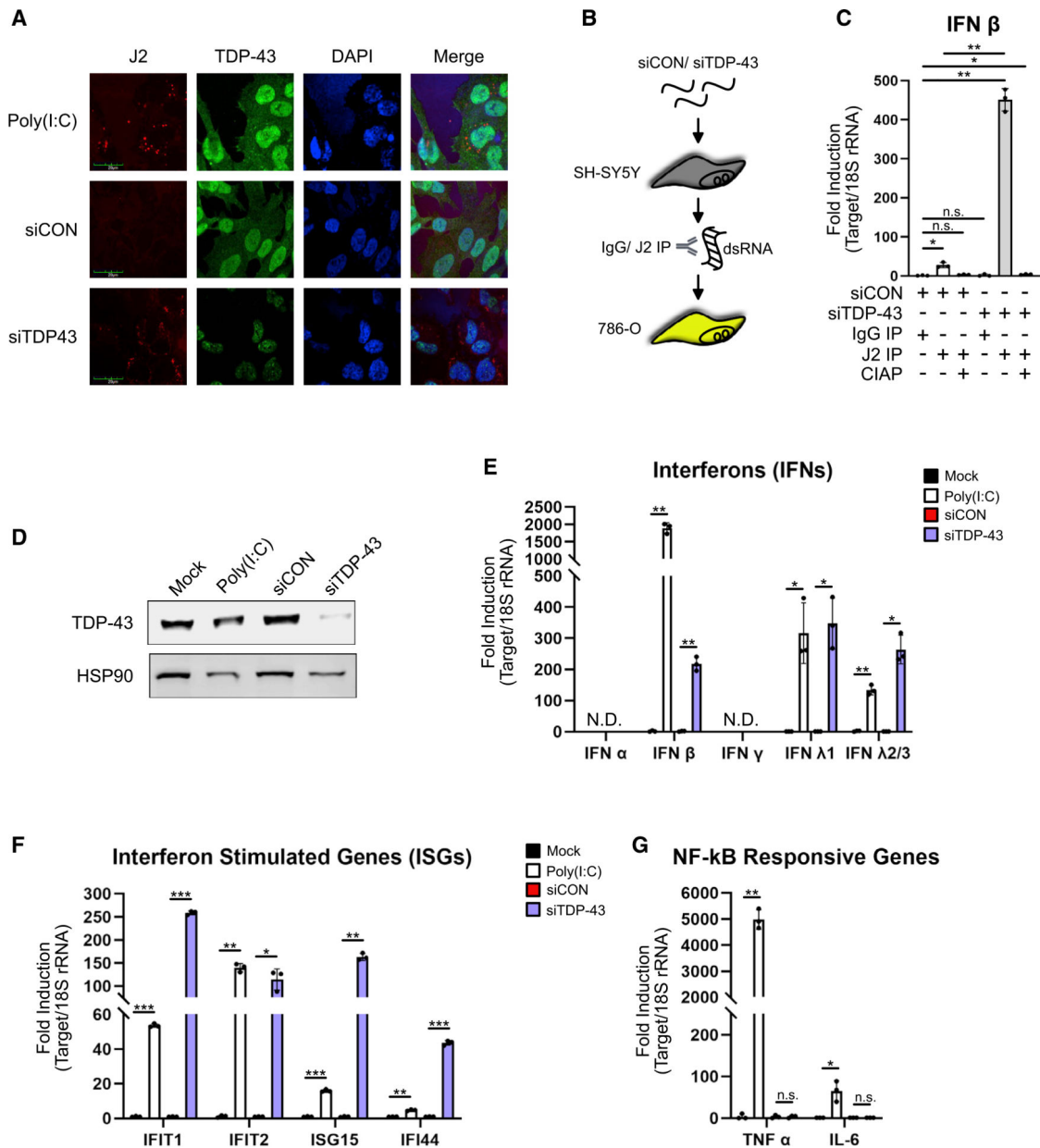
Figure 1. TDP-43 depletion induces cytoplasmic immunostimulatory dsRNA accumulation and a type-I and -III interferon response

(A) Immunofluorescence microscopy of SH-SY5Y cells treated with siCON/siTDP-43 for 48 h. Poly(I:C) was transfected as a dsRNA positive control. Scale bars: 20 μm.

(B) Schematic of IgG/J2 immunoprecipitation (IP) from siCON/siTDP-43-treated SH-SY5Y cells, followed by transfection into 786-O cells.

(C) qRT-PCR analysis of IFN-β levels from 786-O cells transfected with IgG/J2-immunoprecipitated dsRNA for 24 h. J2-purified RNA was either mock or CIAP treated before transfection. siCON IgG was set to 1.

(D) Western blot analysis of SH-SY5Y cells treated with siCON/siTDP-43 for 48 h.

(E–G) qRT-PCR analysis of interferons (IFNs).

(E) Interferon-stimulated genes (ISGs) (F), and NF-κB-responsive genes (G) from cells in (D).

All samples were normalized to 18S rRNA, and mock/siCON levels were set to 1. Student's t test was used to determine statistical significance: *p 0.05, **p 0.005, ***p 0.0005; ns, not significant. (C) n = 2 and (E–G) n = 3 biological replicates, and representative qPCR with technical triplicates is shown.

See also Figure S1.
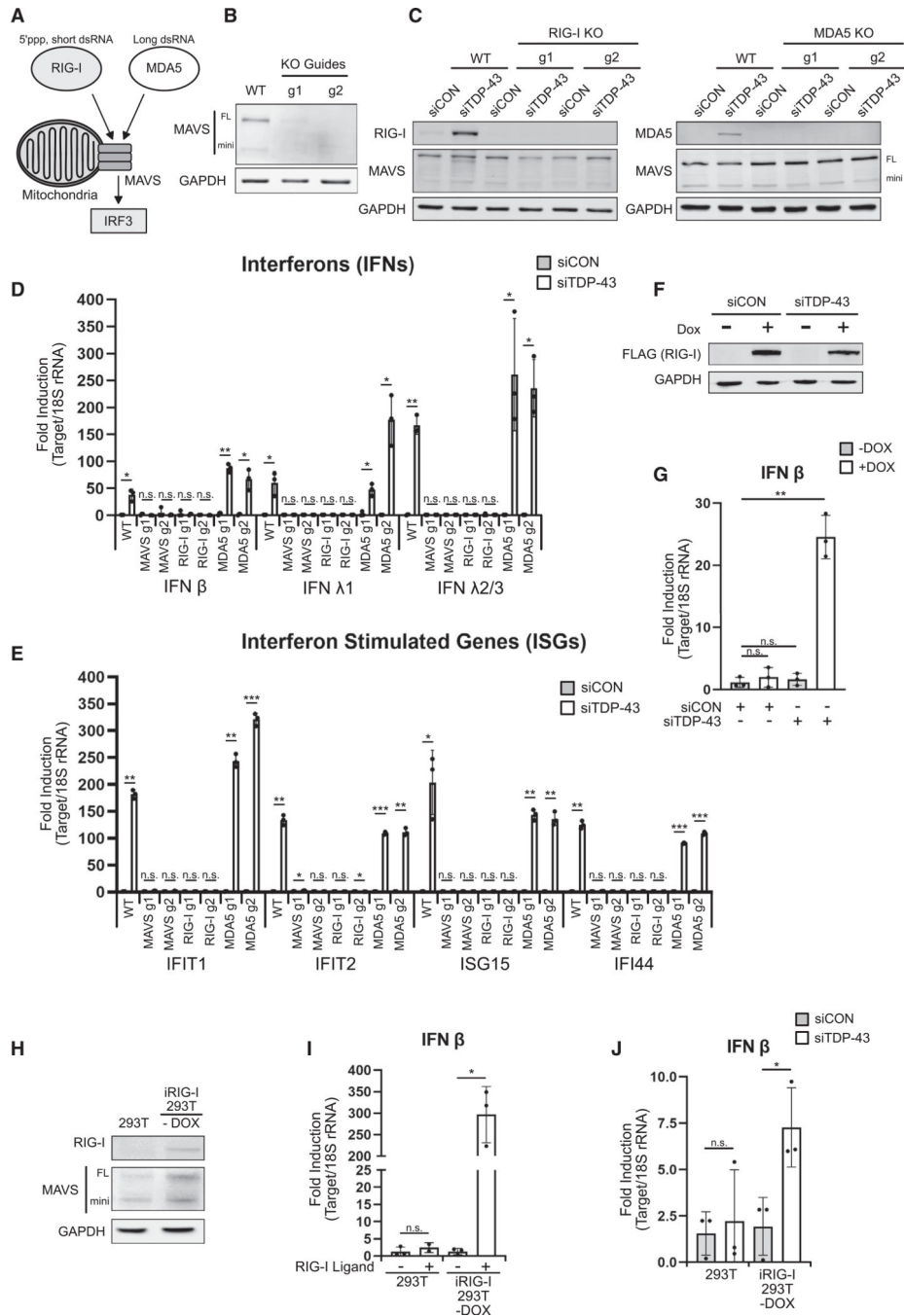
Figure 2. TDP-43 knockdown activates a RIG-I- and MAVS-dependent interferon response

(A) Schematic of RIG-I-like receptor (RLR) signaling pathway.

(B) Western blot analysis of SH-SY5Y MAVS knockout (KO) cells. Two independent-guide RNAs are shown, and full length (FL) and mini-MAVS (mini) are depicted.

(C) Western blot analysis of SH-SY5Y RIG-I and MDA5 KO cells. Cells were treated with siCON/siTDP-43 for 48 h.

(D and E) qRT-PCR analysis of IFNs (D) and ISGs (E) after siCON/siTDP-43 treatment for 48 h.

(F) Western blot analysis of SH-SY5Y RIG-I KO cells complemented with DOX-inducible, FLAG-tagged RIG-I. Cells were treated with siCON/siTDP-43 for 48 h and with DOX for the final 24 h.

(G) qRT-PCR analysis of IFN-β levels from cells in (F).

(H) Western blot analysis of HEK293T and DOX-inducible RIG-I (iRIG-I) HEK293T cells.

(I) qRT-PCR analysis of IFN-β levels after RIG-I ligand transfection into cells in (H) for 6 h.

(J) qRT-PCR analysis of IFN-β levels after siCON/siTDP-43 treatment of HEK293T and iRIG-I HEK293T cells for 48 h.

All samples were normalized to 18S rRNA, and siCON/ Mock levels were set to 1. Student's t test was used to determine statistical significance: *p 0.05, **p 0.005, ***p 0.0005; ns, not significant. (n = 3 biological replicates, and representative qPCR with technical triplicates is shown).

See also Figures S2 and S3.
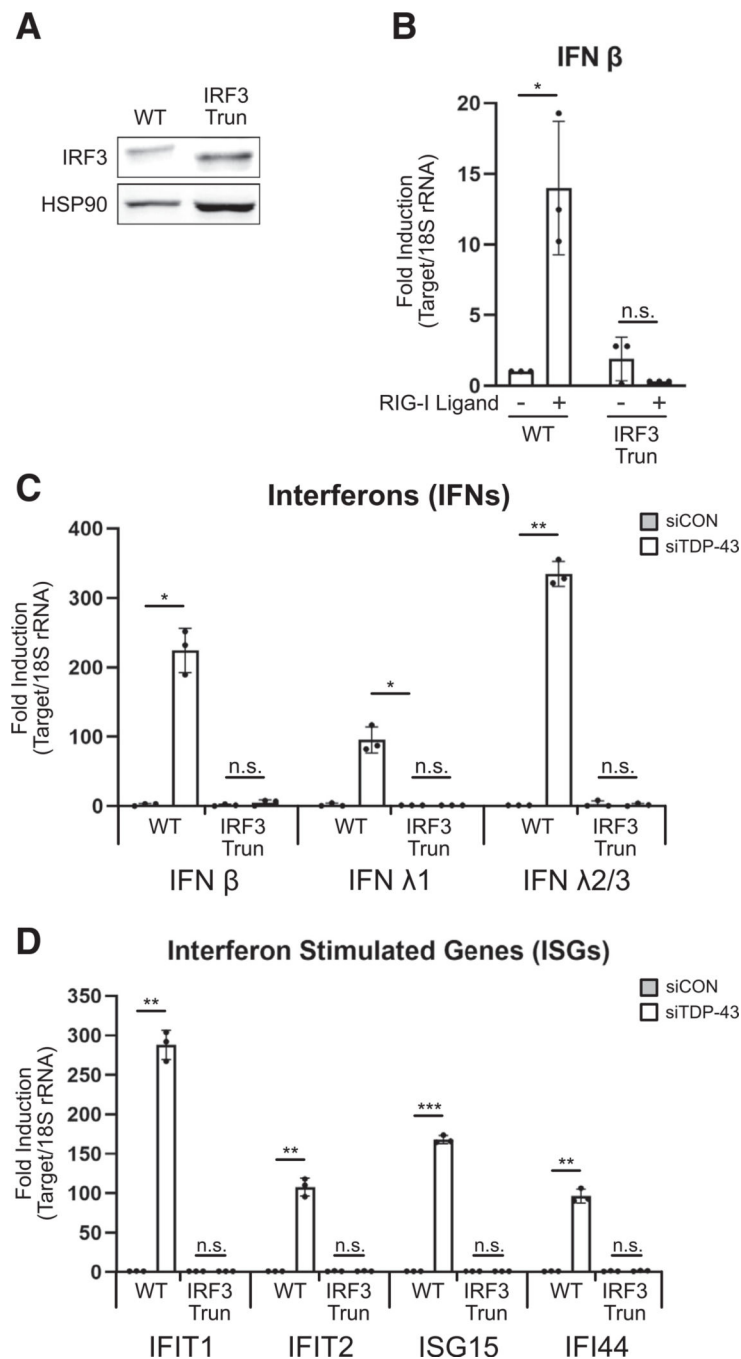
Figure 3. IRF3 is responsible for the TDP-43-depletion-induced interferon response

(A) Western blot analysis of truncated IRF3 (IRF3 trun) cells.

(B) qRT-PCR analysis of IFN b levels after RIG-I ligand transfection for 6 h.

(C and D) qRT-PCR analysis of IFN (C) and ISG (D) levels after siCON/siTDP-43 treatment for 48 h.

All samples were normalized to 18S rRNA and mock/siCON levels were set to 1. Student's t test was used to determine statistical significance: *p 0.05, **p 0.005, ***p 0.0005;

ns, not significant. (n = 3 biological replicates, and representative qPCR with technical triplicates is shown).
See also Figure S4.
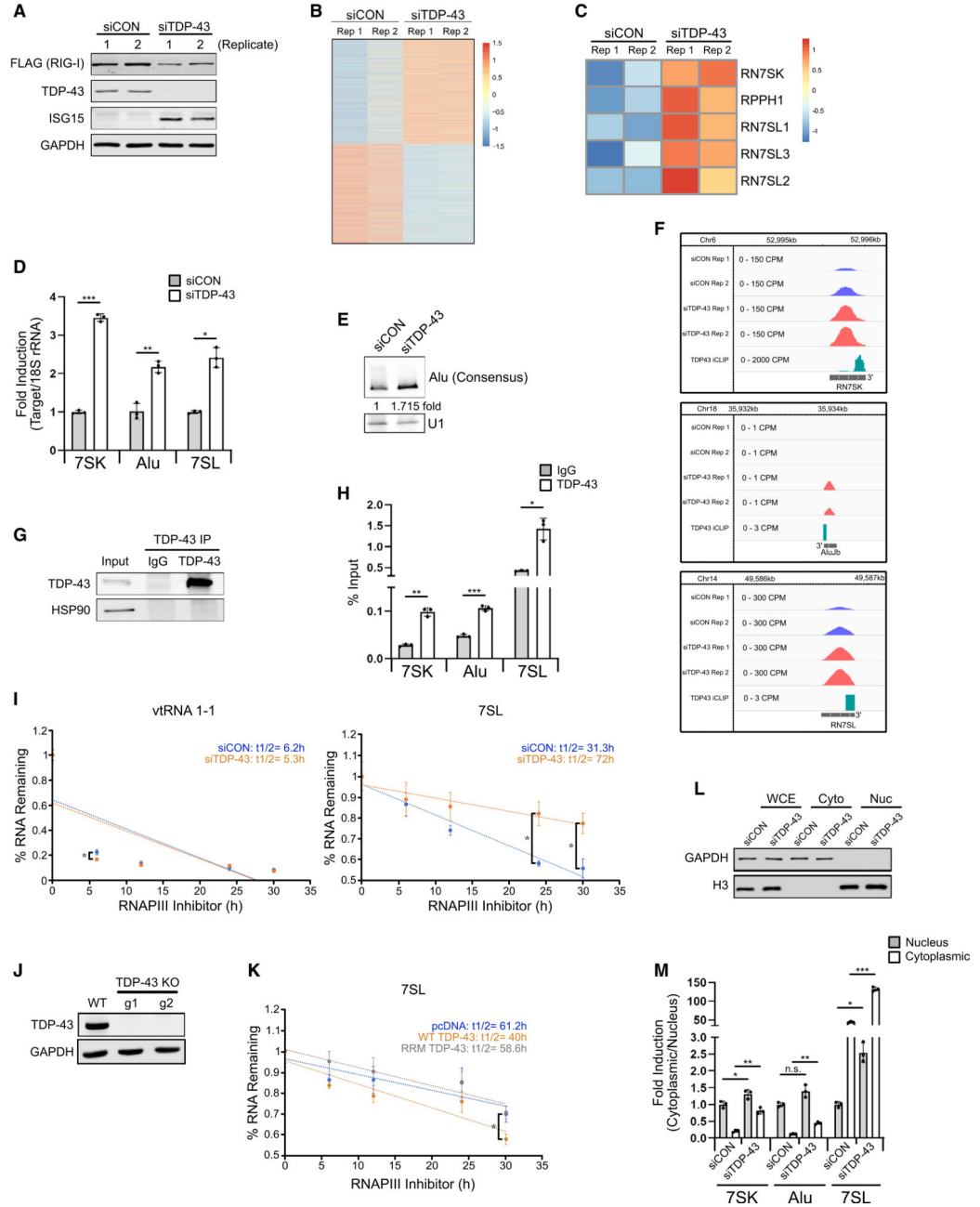
Figure 4. TDP-43 represses RNAPIII-transcribed RNAs to prevent cytoplasmic relocalization

(A) Western blot analysis of SH-SY5Y RIG-I complement cells treated with siCON/siTDP-43 for 48 h and with DOX treatment for 24 h. Two replicates are shown for each condition.

(B and C) Heatmap of global up- and downregulated transcripts (B) and RNAPIII-transcribed genes (C) from (A).

(D) qRT-PCR analysis of RNAPIII transcripts from SH-SY5Y cells treated with siCON/siTDP-43. Samples were normalized to 18S rRNA, and siCON levels were set to 1.

Figure 5. Induced RNAPIII transcripts bind RIG-I to activate an IFN response that is rescued by exogenous TDP-43 expression in an RNA binding-dependent manner

(A) qRT-PCR analysis of vault RNA (vtRNA) 1–1 and IFN-β levels after siCON/siTDP-43 and RNAPIII inhibitor treatment for 24 h.

(B and C) Western blot analysis (B) and qRT-PCR analysis (C) of HEK293T TDP-43 KO cells transfected with FLAG-tagged RIG-I and FLAG-tagged TDP-43 plasmids for 24 h.

(D and E) Western blot analysis (D) and qRT-PCR analysis (E) of bound RNAs from FLAG-RIG-I IP of SH-SY5Y RIG-I complement cells treated with siCON/siTDP-43 for 48 h and

DOX treatment for 24 h. Fold enrichment was computed by the percentage of input, and siCON was set to 1.

(F and G) Western blot analysis (F) and qRT-PCR analysis (G) of DOX-inducible FLAG-DUSP11 treated with siCON/siTDP-43 and DOX for 48 h.

All samples were normalized to 18S rRNA and mock/siCON levels were set to 1. Student's t test was used to determine statistical significance: *p   0.05, **p   0.005, ***p   0.0005; ns: not significant. (A and G) n = 2; (C and E) n = 3 biological replicates, and representative qPCR with technical triplicates is shown.
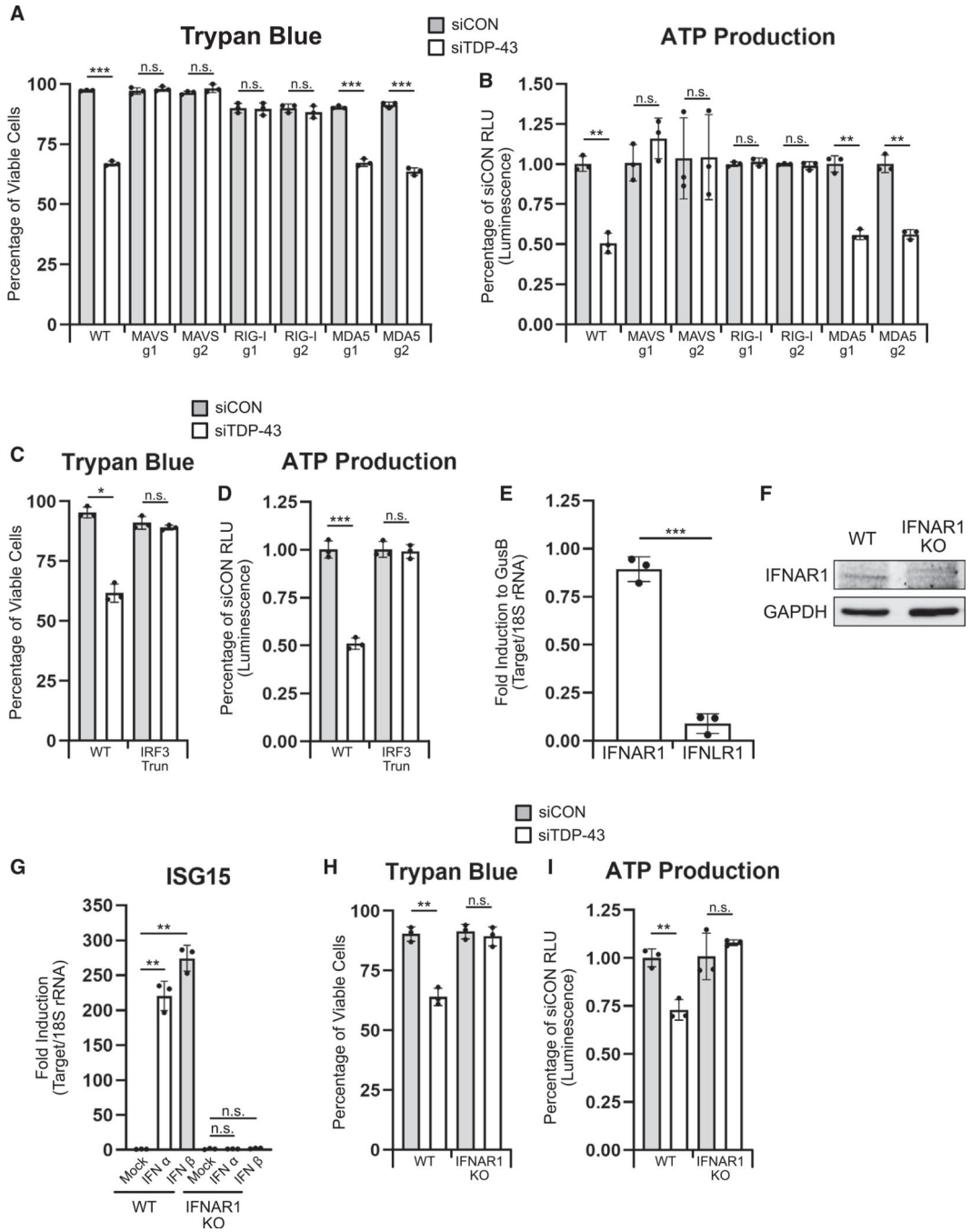
Figure 6. TDP-43 depletion-induced cell death requires activation of the RLR signaling pathway and type-I interferon signaling

(A and B) Trypan blue staining (A) and CellTiter-Glo analysis (B) of SH-SY5Y KO cells treated with siCON/siTDP-43 for 96 h.

(C and D) Trypan blue staining (C) and CellTiter-Glo (D) of SH-SY5Y truncated IRF3 cells similar to (A) and (B).

(E) qRT-PCR analysis of IFNAR1 and IFNLR1 levels from SH-SY5Y cells. All samples were normalized to 18S rRNA, followed by the housekeeping gene GusB, where GusB levels were set to 1.

(F) Western blot analysis of IFNAR1 KO SH-SY5Y cells.

(G) qRT-PCR analysis of ISG15 levels from WT and IFNAR1 KO SH-SY5Y cells treated with IFN-α or -β for 8 h. Mock levels were set to 1.

(H and I) Trypan blue staining (H) and CellTiter-Glo analysis (I) of SH-SY5Y IFNAR1 KO cells similar to (A) and (B).

Student's t test was used to determine statistical significance: *p 0.05, **p 0.005, ***p 0.0005; ns: not significant. (n = 3 biological replicates, and representative qPCR with technical triplicates is shown; n = 3 biological replicates for all trypan blue and CellTiter-Glo experiments).

See also Figure S5.
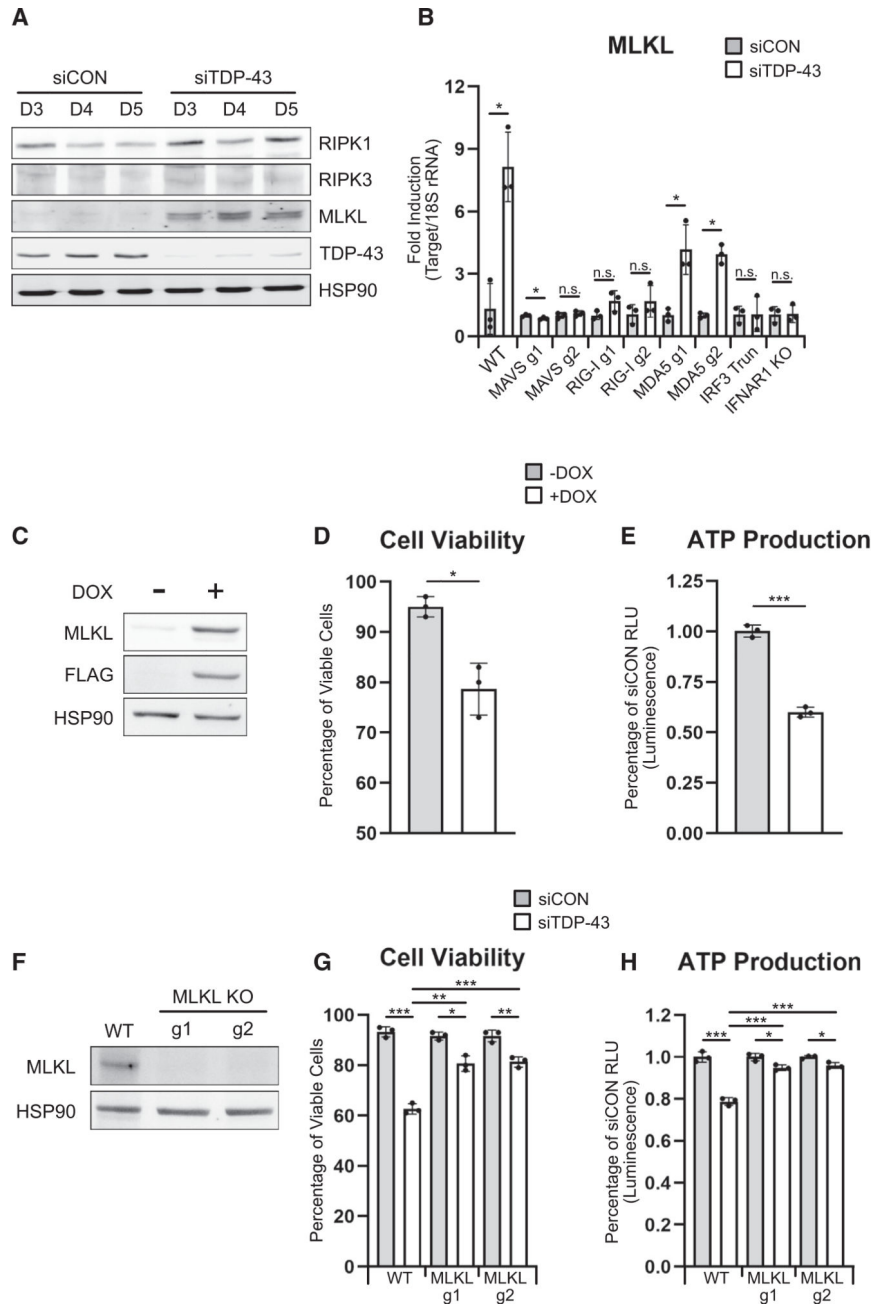
Figure 7. TDP-43 knockdown induces MLKL overexpression to activate necroptosis

(A) Western blot analysis of MLKL levels from SH-SY5Y cells treated with siCON/ siTDP-43.

(B) qRT-PCR analysis of MLKL levels from SH-SY5Y WT and KO cells treated with siCON/siTDP-43 for 48 h. All samples were normalized to 18S rRNA, and siCON levels were set to 1.

(C) Western blot of inducible MLKL SH-SY5Y cells where doxycycline was added for 24 h.

(D and E) Trypan blue staining (D) and CellTiter-Glo analysis (E) of cells in (D). DOX was added for 48 h.

(F) Western blot of MLKL KO SH-SY5Y cells.

(G and H) Trypan blue staining (G) and CellTiter-Glo analysis (H) of MLKL KO cells treated with siCON/siTDP-43 for 96 h.

Student's t test was used to determine statistical significance: *p 0.05, **p 0.005, ***p 0.0005; ns, not significant. (n = 3 biological replicates, and representative qPCR with technical triplicates is shown; n = 3 biological replicates for all trypan blue and CellTiter-Glo experiments).

See also Figure S6.

Author Manuscript Author Manuscript Author Manuscript Author Manuscript

KEY RESOURCES TABLE

REAGENT or RESOURCE	SOURCE	IDENTIFIER
Antibodies		
Rabbit polyclonal anti-HSP90	Cell Signaling Technology	Cat# 4874S
Mouse monoclonal anti-GAPDH	Proteintech	Cat# 60004-I-Ig
Rabbit monoclonal anti-IRF3	Cell Signaling Technology	Cat# 4302S
Rabbit monoclonal anti-MDA5	Cell Signaling Technology	Cat# 5321S
Mouse monoclonal anti-FLAG	Sigma	Cat# F1804-200UG
Rabbit polyclonal anti-IFNAR1	Proteintech	Cat# 13083-I-AP
Rabbit monoclonal anti-MLKL	Cell Signaling Technology	Cat# 14993T
Rabbit monoclonal anti-H3	Millipore	Cat# 05-928
Rabbit polyclonal anti-TDP-43	Proteintech	Cat# 10782-2-AP
Rabbit monoclonal anti-RIG-I	Abcam	Cat# ab180675
Mouse monoclonal anti-ISG15	Santa Cruz Biotechnology	Cat# sc-166755
Rabbit polyclonal anti-MAVS	Bethyl	Cat# A300-782A
Mouse monoclonal anti-J2	Scicons	https://scicons.eu/en/antibodies/j2/
Anti-rabbit IgG AlexaFluor-800	Invitrogen	Cat# A32735
Anti-rabbit IgG AlexaFluor-680	Invitrogen	Cat# A32734
Anti-mouse IgG AlexaFluor-800	Invitrogen	Cat# A32730
Anti-mouse IgG AlexaFluor-680	Invitrogen	Cat# A32729
Anti-mouse IgG Rhodamine Red-X	Invitrogen	Cat# R6393
Anti-rabbit IgG Cyanine5	Invitrogen	Cat# A10523
Control IgG	Sigma	Cat# I5006
Rabbit monoclonal anti-RIPKI	CST	Cat# 3493T
Rabbit monoclonal anti-RIPK3	CST	Cat# 13526T
Bacterial and virus strains		
KSHV virions from iSLK.BAC16	Brulois et al., 2012	N/A
Chemicals, peptides, and recombinant proteins		
Doxycycline	Fisher	Cat# BP2653-1
Lipofectamine RNAiMAX	Invitrogen	Cat# 13778-150
Poly-L-Lysine	Sigma	Cat# P8920-100mL
Paraformaldehyde	Ted Pella	Cat# 18505
Triton X-100	VWR	Cat# 0694-1L
Bovine Serum Albumin	Rockland	Cat# BSA-1000
Normal Goat Serum	Life Technologies	Cat# 50062Z
Tween-20	Fisher	Cat# BP337-500
Mounting Media with DAPI	Invitrogen	Cat# P36931
TRIzol	Invitrogen	Cat# 15596018
DNase I	NEB	Cat# M0303S

REAGENT or RESOURCE	SOURCE	IDENTIFIER
EDTA	RPI	Cat# E57020-500
Tris Base	VWR	Cat# 0497-5KG
NaCl	Fisher	Cat# S271-10
NP-40	Alfa Aesar	Cat# J61055
MgCl2	Sigma	Cat# M2670500G
Ribo-lock	Thermo	Cat# EO0381
SureBeads Protein G Magnetic Beads	Bio-Rad	Cat# 161-4023
M-MLV RT	Promega	Cat# M170A
PVDF	Millipore	Cat# IPFL00010
PEG	VWR	Cat# 0159-500G
Polybrene	Millipore	Cat# TR-1003-G
Polyjet	SignaGen	Cat# SL100688
Hygromycin B	Invitrogen	Cat# 10687010
Blasticidin	GIBCO	Cat# A11139-03
Puromycin	Sigma	Cat# P8833
3p-hpRNA	Invivogen	Cat# tlrl-hprna
IFN Alpha	Sigma	Cat# SRP4596
IFN Beta	Peprotech	Cat# 300-02BC
Formaldehyde	VWR	Cat# M134-500ML
Glycine	RPI	Cat# G36050-1000
KCl	Fisher	Cat# BP366-1
DTT	VWR	Cat# 0281-5G
SDS	VWR	Cat# M107-500G
Anti-FLAG M2 Magnetic Beads	Sigma	Cat# M8823-5ML
Urea	Fisher	Cat# U15-3
1X FLAG Peptide	Sigma	Cat# F3290
Phenol:chloroform	VWR	Cat# 0883-400mL
Trypan Blue	Corning	Cat# 25-900-CI
Dulbecco's modified Eagle medium (DMEM)	Corning	Cat# 10-017-CV
Ham's F-12 nutrient mixture	GIBCO	Cat# 11765-054
Fetal Bovine Serum (FBS)	Invitrogen	Cat# 26140-079
Penicillin/streptomycin	GIBCO	Cat# 15140-122
PowerUP SYBR green	Applied Biosystems	Cat# 100029284
Halt Protease Inhibitor	Thermo	Cat# 1861279
Opti-MEM	GIBCO	Cat# 31985-070
PBS	Corning	Cat# 21-031-CV
Milk	American Bio	Cat# AB10109-01000
Formamide	VWR	Cat# 0606
Bromophenol blue	Sigma	Cat# B0126
Xylene cyanol	Sigma	Cat# X4126
10% TBE-Urea gel	Invitrogen	Cat# EC6875BOX
Sodium phosphate monobasic	Amresco	Cat# 0571

REAGENT or RESOURCE	SOURCE	IDENTIFIER
Sodium deoxycholate	Fisher	Cat# BP349
CAS 577784-91-9	Millipore	Cat#557403
Sodium phosphate dibasic	VWR	Cat# 0404
CIAP	Promega	Cat# M182A
Critical commercial assays		
QIAquick Gel Extraction Kit	QIAGEN	Cat# 28706
QIAprep Spin Miniprep Kit	QIAGEN	Cat# 27106
Bradford Protein Assay Dye	Bio-Rad	Cat# 5000006
TOPO TA Cloning Kit	Thermo	Cat # 450641
Gateway BP Clonase II	Invitrogen	Cat# 11789100
Gateway LR Clonase II	Invitrogen	Cat# 11791020
NEBNext rRNA Depletion Kit	NEB	Cat# E6310
Collibri Stranded RNA Library Prep Kit	Invitrogen	Cat# A38994024
CellTiter-Glo 2.0	Promega	Cat# G9241
Kapa HiFi HotStart PCR Kit	Kapa Biosystems	Cat# KR0369
Deposited data		
SH-SY5Y siCON/siTDP-43 RNA Seq	This paper	GEO: GSE162644
SH-SY5Y iCLIP	Tollervey et al., 2011	E-MTAB-530
Experimental models: Cell lines		
SH-SY5Y	ATCC	Cat# CRL-2266
786-O	ATCC	Cat# CRL-1932
HEK293T	ATCC	Cat# CRL-3216
iSLK.BAC16	Brulois et al., 2012	N/A
Oligonucleotides		
See Table S1 for siRNA Sequences, qPCR Oligos, Cloning Oligos, and Northern Blot Probes		N/A
Recombinant DNA		
Plasmid: lentiCRISPR V2	Addgene	Cat# 52961
Plasmid: Scr lentiCRISPR V2	This Paper	N/A
Plasmid: MAVS KO lentiCRISPR V2	This Paper	N/A
Plasmid: RIG-I KO lentiCRISPR V2	This Paper	N/A
Plasmid: MDA5 KO lentiCRISPR V2	This Paper	N/A
Plasmid: psPAX2	Addgene	Cat# 12260
Plasmid: pMD2.G	Addgene	Cat# 12259
Plasmid: RIG-I pLenti-CMVtight-FL-HA-DEST-Blast	Zhao et al., 2018	N/A
Plasmid: pLenti CMV rtTA3 Hygro	Addgene	Cat# 26730

REAGENT or RESOURCE	SOURCE	IDENTIFIER
Plasmid: pEF-Bos FLAG-RIG-I	Addgene	Cat# 52877
Plasmid: pLenti-CMV-tight-blast-dest	Addgene	Cat# 26434
Plasmid: IRF3 KO lentiCRISPR V2	This Paper	N/A
Plasmid: IFNAR1 KO lentiCRISPR V2	This Paper	N/A
Plasmid: MLKL pF-TRE3G-PGK-puro	Petrie et al., 2018	N/A
Plasmid: TDP-43 KO lentiCRISPR V2	This Paper	N/A
Plasmid: DUSP11 pLenti-CMVtight-FL-HA-DEST-Blast	This Paper	N/A
Plasmid: MLKL pLenti-CMVtight-FL-HA-DEST-Blast	This Paper	N/A
Plasmid: FLAG-TDP-43 pcDNA3 WT	Freibaum et al., 2010	N/A
Plasmid: FLAG-TDP-43 pcDNA3 mutRRM	Freibaum et al., 2010	N/A
Plasmid: MLKL KO lentiCRISPR V2	This Paper	N/A
Software and algorithms		
STAR (v2.7.3a)	https://github.com/alexdobin/STAR	version 2.7.3a
featureCounts	http://bioinf.wehi.edu.au/featureCounts/	version 2.0.0
edgeR (v2.26.5)	https://www.bioconductor.org/packages/release/bioc/html/edgeR.html	version 2.26.5
clusterProlifer (v3.12.0)	https://bioconductor.org/packages/release/bioc/html/clusterProfiler.html	version 3.12.0
R package stats (kmeans)	https://stat.ethz.ch/R-manual/R-devel/library/stats/html/00Index.html	version 4.1.0
pheatmap (v1.0.12)	https://github.com/raivokolde/pheatmap	version 1.0.12
FastQC (v0.11.5)	https://www.bioinformatics.babraham.ac.uk/projects/fastqc/	version 0.11.5